Redox Biology 21 (2019) 101049

Contents lists available at ScienceDirect

Redox Biology

journal homepage: www.elsevier.com/locate/redox

Research Paper

Thioredoxin and glutaredoxin regulate metabolism through different multiplex thiol switches

MJ López-Grueso[a,e], R González-Ojeda[b], R Requejo-Aguilar[a,e], B McDonagh[c], CA Fuentes-Almagro[d], J. Muntané[c], J.A. Bárcena[a,e,*], CA Padilla[a,e]

[a] Dept. Biochemistry and Molecular Biology, University of Córdoba, Córdoba, Spain
[b] Institute of Biomedicine of Seville (IBIS), IBiS/"Virgen del Rocío" University Hospital/CSIC/University of Seville, Seville, Spain
[c] Dept. of Physiology, School of Medicine, NUI Galway, Ireland
[d] SCAI, University of Córdoba, Córdoba, Spain
[e] Maimónides Biomedical Research Institute of Córdoba (IMIBIC), Córdoba, Spain

ARTICLE INFO

Keywords:
Redox proteome
Thiol redox regulation
Glycolysis
S-nitrosation
NO synthase
Redoxins

ABSTRACT

The aim of the present study was to define the role of Trx and Grx on metabolic thiol redox regulation and identify their protein and metabolite targets. The hepatocarcinoma-derived HepG2 cell line under both normal and oxidative/nitrosative conditions by overexpression of NO synthase (NOS3) was used as experimental model. Grx1 or Trx1 silencing caused conspicuous changes in the redox proteome reflected by significant changes in the reduced/oxidized ratios of specific Cys's including several glycolytic enzymes. Cys^{91} of peroxiredoxin-6 (PRDX6) and Cys^{153} of phosphoglycerate mutase-1 (PGAM1), that are known to be involved in progression of tumor growth, are reported here for the first time as specific targets of Grx1. A group of proteins increased their Cys_{RED}/Cys_{OX} ratio upon Trx1 and/or Grx1 silencing, including caspase-3 Cys^{163}, glyceraldehyde-3-phosphate dehydrogenase (GAPDH) Cys^{247} and triose-phosphate isomerase (TPI) Cys^{255} likely by enhancement of NOS3 autooxidation. The activities of several glycolytic enzymes were also significantly affected. Glycolysis metabolic flux increased upon Trx1 silencing, whereas silencing of Grx1 had the opposite effect. Diversion of metabolic fluxes toward synthesis of fatty acids and phospholipids was observed in siRNA-Grx1 treated cells, while siRNA-Trx1 treated cells showed elevated levels of various sphingomyelins and ceramides and signs of increased protein degradation. Glutathione synthesis was stimulated by both treatments. These data indicate that Trx and Grx have both, common and specific protein Cys redox targets and that down regulation of either redoxin has markedly different metabolic outcomes. They reflect the delicate sensitivity of redox equilibrium to changes in any of the elements involved and the difficulty of forecasting metabolic responses to redox environmental changes.

1. Introduction

The importance of redox homeostasis for cancer cell survival in the context of energy metabolism is well established [2,57,83]. Sensitive cysteine residues on target proteins are at the center of regulatory mechanisms, whose redox state are controlled by two major cellular systems, the Thioredoxin (Trx)/Trx reductase (TrxR) and the Glutaredoxin (Grx)/glutathione (GSH) systems [30,8].

Nitric oxide (NO) plays important roles in signal transduction [52]. It is synthesized in cells by NO synthase (NOS) isoenzymes whose expression may be regulated as part of cellular responses to several stimuli [1]. NO has contradictory effects on tumor cells, either pro-apoptotic or anti-apoptotic according to cell type, intracellular concentration range and subcellular site of its generation [23,44]. Post-translational redox modifications (redox PTM) of target sensitive proteins and more specifically, S-nitrosation of sensitive cysteine residues in those proteins, is the basis of NO activity in signaling pathways, although other reversible oxidative modifications of cysteines are also to be expected since high levels of NO are accompanied by increased levels of reactive oxygen species (ROS) [85]. Reversible regulation of redox PTMs is necessary for this process to have regulatory and biological meaning. Intracellular levels of GSNO and S-nitrosated proteins are controlled by GSNO reductase, alcohol dehydrogenase class-3 (ADH III), which is a NADH-dependent enzyme that is conserved from bacteria to human and metabolizes GSNO to oxidized glutathione and NH_3 [47]. GSNO reductase does not directly denitrosate SNO proteins, but as

* Correspondence to: Dep. of Biochemistry and Molecular Biology, Campus de Rabanales, Ed. Severo Ochoa, 1ª Pl. University of Córdoba, 14071 Córdoba, Spain.
E-mail address: ja.barcena@uco.es (J.A. Bárcena).

https://doi.org/10.1016/j.redox.2018.11.007
Received 5 October 2018; Received in revised form 8 November 2018; Accepted 11 November 2018
Available online 16 November 2018

the GSNO pool is in equilibrium with protein thiols, reduction of GSNO by the GSNO reductase indirectly results in protein denitrosation [47].

Trx has been shown to catalyze denitrosation in vitro and to affect levels of cellular protein nitrosothiols. It has been shown to also catalyze the direct denitrosation of proteins in vivo through the action of its conserved active site dithiol, which in human Trx1 is Cys32 and Cys35 [4,5]. NOS3 (or eNOS) itself is a target of Trx leading to activation of the enzyme as part of a regulatory mechanism of NOS3 by reversible auto-S-nitrosation [15,4,64,67].

Mammalian Trx1 contains additional conserved Cys at positions 62, 69 and 73. Cys73 is particularly prone to S-nitrosation [26] and is implicated in the specific and reversible transfer of a nitrosothiol between Trx1 and caspase 3 with the resulting inhibition of apoptosis [60]. It has been shown that S-nitrosation of Cys73 is favored after formation of a disulfide between Cys32-Cys35, that attenuates Trx1 disulfide reductase and denitrosase activities [86]. Depending on the redox state of the cell, Trx1 catalyzes either trans-S-nitrosation or S-denitrosation so that upon inhibition of disulfide reduction or S-denitrosation activity, Cys^{73}-SNO-Trx1 could catalyze trans-S-nitrosation of target proteins [26,86]. Thus, as a master regulator of redox signaling, Trx1 would protect proteins via its reductase activity, but under highly oxidative environments, the Cys32/Cys35 oxidized disulfide form accumulates, Cys73 becomes S-nitrosated and Trx1 offers an alternative modality of protein regulation via transnitrosation [86].

Glutaredoxin is involved in post-translational modification of proteins by S-glutathionylation with a role mainly as a deglutathionylase [39,54,75]. Grx1 catalyzes reversible S-glutathionylation of protein targets involved in Glycolysis, energy sensing, calcium homeostasis, apoptosis and transcriptional regulation [59]. Grx1 has also been shown to counteract the proapoptotic action of NO in tumor cell lines [22,35] and to regulate NOS3 activity by glutathionylation [9], an activity shared with Trx [78]. However, no direct evidence of Grx1 as denitrosase has been reported so far.

The thiol-based mechanism of NO multiple actions and the roles of Trx and Grx in the context of protein function regulation by reversible redox changes at target cysteines justify the study of cells under nitrosative stress. Exogenous addition of NO donors is a widely used experimental approach to this end, but endogenously produced RNS would better mimic a physiological situation. The levels of ROS and NO increase to 140% in NOS3 overexpressing HepG2 cells relative to control cells [21], which makes them a good experimental model to study the significance of Trx and Grx roles in the regulation of cellular physiology under nitrosative and oxidative conditions.

The Thiol Redox Proteome refers to the set of mapped protein cysteines showing reversible redox changes under given conditions or in response to stimuli [20]. Its detailed description may provide an insightful snapshot of the set of thiol redox switches [19,38] in a cell under given conditions. Several qualitative and quantitative proteomic approaches have been devised to study the redox proteome [24,27,32,43,46,50,53,55] and to define Trx target proteins either as reductase or transnitrosase [46,6,87] or target proteins of Grx as deglutathionylase [54]. The identification and modulation by reversible redox PTMs of key proteins that can control metabolic flow, would offer promising therapeutic candidates for a number of disease states such as cancer [80]. Moreover, redox signals work in tandem with other signals to control different cellular processes.

One common characteristic to all types of cancers is reprogramming of energy metabolism to generate ATP through intense glycolytic flux from glucose to lactate even when oxygen is present, a phenomenon known as “the Warburg effect”. Mitochondria remain functional and part of the glucose consumed is diverted into biosynthetic pathways upstream of pyruvate. Altered cell metabolism is a characteristic feature of many cancers resulting in changes to metabolite concentrations and eventually affecting cell signaling pathways and metabolic fluxes [79,83]. There is a complex connection between metabolism and proliferation with many checkpoints still to be discovered.

We have previously assessed the role of NOS-3 overexpression on several metabolic checkpoints in HepG2 cells showing the prominence of the oxidative branch of the Pentose Phosphate Pathway (oxPPP) to direct the metabolic flux towards NADPH and the increase in Trx and Grx, but at the same time a decrease in nucleotide biosynthesis and proliferation [23]. Downregulation of Trx and Grx reduced cell proliferation and increased caspase-8 and caspase-3.

Here we have applied a quantitative proteomic and metabolomic approach to evaluate HepG2 cells under high levels of endogenous NO and ROS by NOS3 overexpression and ≈ 80% down-regulation of Grx1 or Trx1 with specific siRNA. Proteins undergoing significant redox changes have been identified, their sensitive cysteines have been mapped and their “reduced Cys/oxidized Cys” ratios have been determined. Known targets of redox PTMs have been confirmed and new targets have been discovered, mostly metabolic enzymes. Glycolytic metabolic flux, complex lipids and glutathione metabolism and protein degradation, among other pathways, were affected by Trx1 or Grx1 silencing, concomitant with redox changes at specific cysteines in glycolytic enzymes.

2. Material and methods

2.1. Materials and reagents

All reagents were of analytical grade and were purchased from Sigma, unless otherwise stated. HepG2 cell line used in this work was obtained from ATCC LGC Standards Company (Teddington, UK). Cell culture dishes and flasks were from TPP (Switzerland). Anti-Trx1 and anti-Grx1 were obtained from rabbit in our laboratory. Antibodies against PKM2, caspase-3, NOS-3 and β-actin were from Santa Cruz Biotechnology, (Dallas, TX, USA). Antibodies against PRDX6 were from Abcam (Cambridge, UK). ECL was from GE Healthcare (Wauwatosa, Wisconsin, USA). siRNA for Grx1 and Trx1 were from GE Healthcare Dharmacon (Wauwatosa, Wisconsin, USA). [^{14}C-1]-Glucose, [^{14}C-6]-Glucose and [^{3}H-3]-Glucose were from Perkin Elmer (USA).

2.2. Cell growth conditions

Cells were transfected with the pcDNA/4TO (5100 bp; Invitrogen, Molecular Probes, Inc.) resulting in 4TO control cell line, as well as with the same expression vector containing NOS3 cDNA sequence (3462 bp; NCBI, ImaGenes, full length cDNA clone sequence BC063294) under the control of the cytomegalovirus promoter resulting in 4TO-NOS cell line. Cell lineages 4TO and 4TO-NOS were selected with zeocin (15 mg/L; Invitrogen) as was described by González et al. [21]. Cells were maintained in EMEM Medium (Eagle Minimum Essential Medium), pH 7.4, supplemented with 10% fetal bovine serum, 2.2 g/L $NaHCO_3$, 1 mM sodium pyruvate, 100 U/L penicillin, 100 µg/mL streptomycin, 0.25 µg/mL amphotericin, and the corresponding selective zeocin antibiotic in 5% CO_2 atmosphere at 37 °C.

2.3. Silencing of Trx1 and Grx1

Human Grx1 and Trx1 were down-regulated in non-transfected HepG2 cells (WT), 4TO and 4TO-NOS cells using specific siRNA in 6-well plates (20,000 cells/cm^2) according to the manufacturer's recommendations (Dharmacon, GE Healthcare Life Sciences). Grx and Trx siRNA (25 nmol) were mixed with the transfection reagent DharmaFECT 1, previously pre-incubated with culture medium (antibiotic/antimycotic and serum free), and incubated for 20 min at room temperature. Afterwards, the interference solutions were added to cultured cells for 72 h in 2% culture medium in the absence of antibiotic/antimycotic solution [89]. Silencing of Trx 1 and Grx1 was always checked by Western blot and activity assay to confirm that their levels were reduced by ≈ 80% [22].

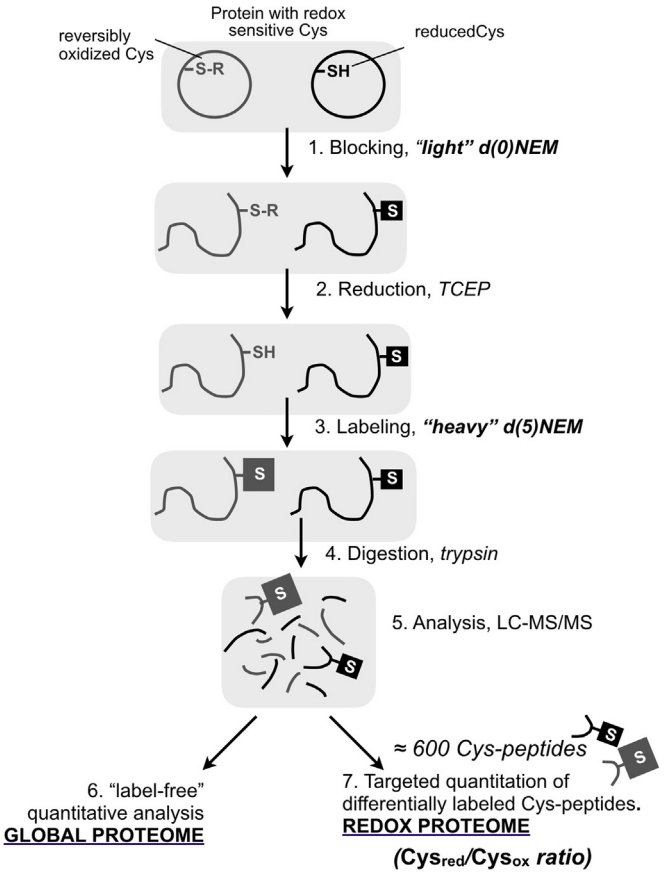

Fig. 1. Proteomics experimental strategy. The procedure follows the already classical three-step approach. In this case, the thiol blocking agent was NEM, the cysteine reductant was TCEP and the newly formed thiols were labeled with "heavy" d(5)-NEM in which 5 hydrogen atoms had been substituted by deuterium atoms. LC-MS/MS data were analyzed for global protein changes with MaxQuant software for "label-free" quantitation [12]. Redox protein changes were analyzed from the set of Cys-peptides identified by targeted quantification using Skyline [48] and calculating the "light"(reduced)/"heavy"(oxidized) Cys ratio. See M&M section for a detailed description.

2.4. Sample preparation for redox proteomics

The experiments were routinely carried out at 100,000 cells/cm^2 and the cells were washed with PBS. The methodological strategy is summarized in Fig. 1 as described before [55]. Reversibly oxidized Cys were labeled with "heavy" NEM in which 5 hydrogen atoms had been substituted by deuterium atoms here named "d(5)NEM" and reduced cysteines were blocked with "light" NEM, here named "d(0)NEM". Cell extracts were obtained with lysis solution (50 mM ammonium bicarbonate, 50 mM d(0)NEM, 0.5% CHAPS, 1 mM PMSF); samples were centrifuged at 15,000*g* for 5 min at 4 °C, excess d(0)NEM was removed using Zeba spin desalting columns (Thermo Scientific). 100 µg of protein were diluted up to 160 µl with 25 mM ammonium bicarbonate, incubated with denaturing reagent by addition of 10 µl of 1% w/v RapiGest (Waters) in 25 mM ammonium bicarbonate, incubated at 80 °C for 10 min and vortexed. 10 µl of a 100 mM solution of TCEP was added followed by incubation at 60 °C for 10 min to reduce the reversibly oxidized cysteines that were subsequently alkylated by adding 10 µl of 200 mM d(5)NEM and incubated at room temperature for 30 min. An aliquot was taken at this point to check the procedure by SDS-PAGE.

Proteolytic digestion was performed by addition of 10 µl 12.5 ng/µl of trypsin (Promega) in 25 mM ammonium bicarbonate and incubated at 37 °C temperature overnight. Protein digestion was stopped by addition of 3 µl trifluoroacetic acid (1.5% final concentration). Digested samples were dialyzed through detergent removal column (Pierce) to eliminate any possible rest of CHAPS and dried in speedvac.

2.5. LC–MS/MS

Protein analyses were performed at the Proteomics Facility (SCAI) at the University of Córdoba. Peptides were scanned and fragmented with the LTQ Orbitrap XL mass spectrometer (Thermo Fisher Scientific) equipped with a nano-UHPLC Ultimate 3000 (Dionex-Thermo Scientifics). Chromatography conditions were: mobile phase solution A: 0.1% formic acid in ultrapure water; mobile phase solution B: 80% acetonitrile, 0.1% formic acid. A chromatography gradient was performed in C18 nano-capillary column (Acclaim PepMap C18, 75 µm internal diameter, 3 µm particle size, Dionex-Thermo Scientifics) as follows: 5 min, 4% solution B; 60 min, 4–35% solution B; 10 min, 35–80% B; 10 min, 80% B; 10 min 4% B. The nano-electrospray voltage was set to 1300 V and the capillary voltage to 50 V at 190 °C. The LTQ Orbitrap XL was operated in parallel mode, allowing for the accurate measurement of the precursor survey scan (400–1500 m/z) in the Orbitrap selection, a 30,000 full-width at half-maximum (FWHM) resolution at m/z 400 concurrent with the acquisition of top five CID Data-Dependent MS/MS scans in the LIT for peptide sequence. Singly charged ions were excluded. The normalized collision energies used were 35% for CID. The maximum injection times for MS and MS/MS were set to 500 ms and 50 ms, respectively. The precursor isolation width was 3 amu and the exclusion mass width was set to 5 ppm. Monoisotopic precursor selection was allowed and singly charged species were excluded. The minimum intensity threshold for MS/MS was 500 counts for the linear ion trap and 1000 counts for the Orbitrap. MS2 spectra were searched with SEQUEST engine against a database of Uniprot_Human_Nov2014 (www.uniprot.org). Peptides were generated from a tryptic digestion with up to one missed cleavage, including NEM and (d5)NEM modification in Cys and methionine oxidation as dynamic modifications. Statistical data were calculated with percolator tool against decoy database using 1% FDR as threshold for significance.

2.6. Label-free MS protein quantification

The analysis of MS raw data of the two studies was performed using the MaxQuant (v1.5.7.0) [12] and Perseus (v1.5.6.0) [82] software. Three RAW data files per sample from 3 separate experiments were analyzed. Proteins were identified by searching raw data against the human UniprotKB/Swiss-Prot protein database (February 2018 version). The modifications NEM and d(5)NEM and methionine oxidation was set as variable modifications for the second study. Cleavage specificity was by trypsin, allowing for a maximum of two missed cleavages, a mass tolerance of 10 ppm for precursors and 0.01 Da for fragment ions. The false discovery (FDR) cut-off for protein identification was 1%. Enabling the "match between runs" option allowed for identification transfer between samples. Similar proteins were grouped, and only unique peptides were used for quantification. Identified from reverse database or contaminants hits proteins were removed prior to further analysis. Finally, the resultant list was analyzed according to the instructions of the software developers [82]. The criteria for considering a differentially expressed protein were that it was identified and quantified using at least two unique peptides; has a fold change of at least 1.5 and had a $P \leq 0.05$ value.

2.7. Targeted analysis of differentially labeled Cys residues

The method devised has been described before [55]. Briefly, Cys-containing peptides detected with identical amino acid sequences and both d(0) and d(5) NEM modifications independently with a confident individual peptide ion score were considered redox peptides. Redox peptides detected from Proteome Discoverer analyses of RAW files were

selected for targeted analysis using *m/z* data and retention times with the open software Skyline [48]. Targeted analysis applying *m/z*, retention times, and fragmentation spectra for peptide selection allowed the calculation of the reduced/oxidized ratio (or d(0)/d(5) NEM) of the Cys residues using the individual parent ion intensities. The individual reduced/oxidized ratio for redox Cys peptides in each sample was used to calculate an average ratio of reduced/oxidized calculated for the specific Cys residues.

2.8. Metabolomic analysis

Metabolomic analyses were performed at Metabolon, NC USA and the samples were prepared following the specific guidelines. Global biochemical profiles were determined in 2×10^6 HepG2 cells collected from different treatment groups (wild type, 4TO and 4TO-NOS cells treated with specific siRNA for Trx and Grx or with non-target siRNA). Each experiment was done four times and the dry cell pellets were immediately frozen in liquid nitrogen and stored at −80 °C until shipment. Samples were prepared using the automated MicroLab STAR® system from Hamilton Company. To remove protein, dissociate small molecules bound to protein or trapped in the precipitated protein matrix, and to recover chemically diverse metabolites, proteins were precipitated with methanol under vigorous shaking for 2 min (Glen Mills GenoGrinder 2000) followed by centrifugation. The resulting extract was divided into five fractions: two for analysis by two separate reverse phase (RP)/UPLC-MS/MS methods with positive ion mode electrospray ionization (ESI), one for analysis by RP/UPLC-MS/MS with negative ion mode ESI, one for analysis by HILIC/UPLC-MS/MS with negative ion mode ESI, and one sample was reserved for backup. Raw data was extracted, peak-identified and QC processed using Metabolon's hardware and software. Peaks were quantified using area-under-the-curve and normalized.

2.9. Biotin switch technique

All operations were performed in darkness and following the protocol described by Martínez-Ruiz et al. [51] with some modifications. Treated cells were resuspended in lysis buffer (50 mM Tris-HCl, pH 7.4, 300 mM NaCl, 5 mM EDTA, 0.1 mM neocuproine, 1% Triton X-100, 1 mM PMSF, 1 μg/mL aprotinin and 2 μg/mL leupeptin) and incubated on ice for 15 min. Samples were centrifuged at 10,000*g*, 4 °C for 15 min and supernatants were collected. Extracts were adjusted to 1.0 mg/mL of protein and were blocked with 4 volumes of blocking buffer (225 mM HEPES, pH 7.2, 0.9 mM EDTA, 90 μM neocuproine, 2.5% SDS and 50 mM NEM) at 37 °C for 30 min with stirring. After blocking, samples were precipitated with cold acetone and pellets were resuspended in HENS buffer (250 mM HEPES, pH 7.2, 1 mM EDTA, 0.1 mM neocuproine, 1% SDS) with 100 mM ascorbate and 1 mM biotin-HPDP and incubated for 1 h at room temperature. Finally, samples were passed through Zeba spin desalting columns (Thermo Scientific Pierce) to eliminate ascorbate and biotinylated proteins were detected by western blot with “anti-biotin”. In addition, the biotinylated proteins were captured with neutravidin-agarose (Pierce) and recovered using 100 mM ß-mercaptoethanol for subsequent Western blot analysis of specific target proteins.

2.10. Rate of glycolysis and Pentose Phosphate Pathway (PPP)

These were measured following the protocol described by Requejo-Aguilar et al. [68] with some modifications. The resuspended cells (1.5×10^5 cells) were incubated in “Elliot” buffer (122 mM NaCl, 11 mM Na_2HPO_4, 0.4 mM KH_2PO_2, 1.2 mM SO_4Mg, 3.1 mM KCl, 1.3 mM $CaCl_2$, pH7.4) in the presence of 5 μCi of D-[3-^{3}H]glucose,(0.5 μCi mL^{-1}of D-[1–^{14}C]glucose or 1 μCi mL^{-1} of [6–^{14}C]glucose and 5 mM D-glucose in sealed vials. The glycolytic flux was measured by assaying the rate of ^3H_2O production from [3-^{3}H]glucose, and the PPP flux as the difference between [1–^{14}C]glucose and [6–^{14}C]glucose incorporated into $^{14}CO_2$. Glucose concentrations in Elliot buffer were measured by enzymatic analysis spectrophotometrically.

2.11. Measurement of enzymatic activities, lactate and protein

All glycolytic enzymatic activities were measured in fresh cell lysates obtained in the absence of reducing agents. Cell lysates were prepared with lysis buffer containing 50 mM HEPES pH 7.2, 2 mM EDTA, 100 mM NaCl, 1% Triton X-100, 1 mM PMSF. Commercial preparations of pure enzymes were used to calibrate the assays and to determine the linear dependence activity range. Pyruvate kinase (PK) and triose phosphate isomerase (TPI) activities were measured according to the method described by Fielek and Mohrenweiser [16] without DTT in the assay mixture. Glyceraldehyde-3-phosphate dehydrogenase (G3PDH) activity was measured as an increase in absorption at 340 nm resulting from reduction of NAD^+ at 25 °C. The reaction mixture contained 130 mM Tris-HCl, pH 8.0, 0.25 mM NAD^+, and 5 mM DL-glyceraldehyde-3-phosphate. Three technical replicates were routinely done for each independent experiment. Lactate concentration in the culture medium after 72 h of treatment with the siRNA Grx1 or siRNA Trx1 was determined by an enzymatic colorimetric assay (505 nm) using the kit Labkit (Chemelex, S.A). Protein concentration was determined by the Bradford method (Bio-Rad) using BSA as standard.

2.12. SDS-PAGE and Western blotting

SDS-PAGE was performed with homogeneous 10% non-reducing gels for detection of biotinylated proteins and 12% Criterium XT Precast Gel (Bio-Rad) for detection of specific proteins (Trx1, PRDX6, PKM2, caspase-3, NOS3). After electrophoresis, proteins were transferred to a nitrocellulose membrane with a semi-dry electrophoretic transfer system (Bio-Rad). The membranes were incubated overnight at 4 °C with the corresponding dilutions of primary antibodies: 1:4000 against biotin, 1:1000 against PRDX6, 1:500 against PKM2, caspase-3 and NOS3, 1:500 against Trx1 and Grx1. Then washed and incubated with the corresponding secondary antibodies conjugated to peroxidase (anti-rabbit, anti-goat or anti-mouse) used at 1:8000 dilution and the chemiluminescent signal was induced by ECL reagent (Thermo-Fisher). Ponceau staining was used as cell protein-loading control and actin was used as reference for quantitative densitometric normalization.

2.13. Statistics

Where appropriate, results are expressed as mean ± SEM of at least three independent experiments. Data were compared using ANOVA with the least significant difference test *post hoc* multiple comparison analysis. The threshold for statistically significant differences was set at $p \leq 0.05$. In the case of Global and Redox Proteome, data were analyzed using Student's T-test comparing control *vs* siRNA treatment. The threshold for this statistically significant differences was set at $q \leq 0.05$ according to the method of Storey [77] using the R-package. In the case of the metabolomic analysis following normalization to Bradford protein concentration and log transformation a mixed model ANOVA was used to identify biochemicals that differed significantly between experimental groups; statistical significance was set at $p \leq 0.05$.

3. Results and discussion

Overexpression of NOS3 in HepG2 cells caused a ≈ 25% increase in ROS, NO and NOS activity compared with the same cells transformed with the empty vector [21] and constituted a physiological model for endogenously oxidative/nitrosative stressed cells to study the role of Trx1 and Grx1. Treatment with Trx1 or Grx1 specific siRNA down-regulated the levels and activities of either redoxin by ≈ 80% (Ref.

Fig. 5 in [22]). These cells were collected and lysed under conditions that allowed blocking of reduced protein thiols with "light" d(0)NEM followed by reduction of reversibly oxidized Cys and labelling with "heavy" d(5)NEM (Fig. 1). Samples were prepared and analyzed by a proteomics LC-MS/MS approach allowing for global "label-free" quantitation and for targeted analysis of differentially labeled Cys-peptides [55,71].

3.1. Global proteome

Quantitative differences between the proteomes of WT, 4TO and 4TO-NOS, treated or not with siRNA-Trx1 and siRNA-Grx1, were determined by "label-free" analysis. The significant differential proteomes were determined from roughly 600 unique proteins identified in each study. Only 14 proteins varied significantly between 4TO-NOS and 4TO HepG2 cells and a smaller number changed upon either siRNA treatment in 4TO or 4TO-NOS cells, as shown in Suppl. File 1.

Overexpression of NOS3 and down-regulation of Trx1 or Grx1 in HepG2 cells has marked phenotypical consequences like slow-down of proliferation and apoptosis exacerbation as previously reported [22]. To investigate whether these phenotypical changes might have been triggered by redox postranslational modification of key proteins, we analyzed the redox proteome.

3.2. Redox proteome

Trx1 and Grx1 main action is to reverse oxidative changes in protein thiols, not only those involved in regulatory postranslational modifications of metabolic and signaling proteins, but also those associated with thiol-dependent ROS scavenging enzymes, like peroxiredoxins. Any change in the levels of either redoxin should have consequences on the redox state of sensitive proteins which could reveal detailed knowledge on their functions. Silencing with specific siRNA provides a gentler experimental approach to mimic physiological down-regulation events compared to a full knockout, although detection of the expected subtle changes in molecular indicators requires precise analytical methods to study the redox proteome.

3.2.1. NOS3 overexpression alters the Redox Proteome

The levels of ROS and NO had been measured in 4TO-NOS cells by standard general methods ($DCFH_2$-DA fluorescence and colorimetric nitrite determination, respectively) showing an increase of 40% in the cells overexpressing NOS3 [21]. Now, the Cys_{red}/Cys_{ox} ratio was determined for every Cys peptide identified/quantified in WT (234/168 peptides), 4TO (411/328 peptides) and 4TO-NOS (366/289 peptides) HepG2 cells. Overlapping of Cys-peptides between samples was 65–68% for identified peptides and 71–77% for quantified peptides (Suppl. Fig. 2). The majority of quantified peptides were in the Cys-SH state with Cys_{red}/Cys_{ox} ratios ranging from nearly 40 to around 2. Ninety-four Cys-peptides underwent significant changes in their Cys_{red}/Cys_{ox} ratios when the cells overexpressed NOS3 compared to cells transfected with empty vector (Fig. 2; Suppl. File 2). Changes were predominantly oxidative, but 13 proteins were ≥ 1.5 fold reduced in the oxidative/nitrosative environment of NOS3 overexpressing cells. Their reductive change could be direct or indirect consequence of the observed marked induction of Trx1 and Grx1 [22], but other perturbations in metabolic and signaling pathways induced by NOS3 overexpression could also be responsible.

The presence of acidic residues around the modified cysteine in these redox target proteins is particularly apparent (Fig. 2B). 77% (10/13) of the proteins showing an increase in their reduced/oxidized Cys ratio had at least one Glu or Asp between positions + 2 and −2, centered on the target cysteine, whereas this percentage was lower (46%; 16/35) for the proteins undergoing an oxidative change. The accumulated content of Asp and Glu in the average protein from the UniProtKB TrEMBL is 11.65%, therefore, the frequency of at least one acidic residue at these positions is markedly higher than expected at random and could be related to the sensitivity of these Cys residues to nitrosative stress induced redox changes.

Taken together, these changes show that NOS3 overexpression exerts oxidative pressure on a number of protein cysteine residues with potential regulatory effects mainly at the level of Glycolysis/gluconeogenesis, protein synthesis and folding, endoplasmic reticulum processes, and cell death and survival (Fig. 2C). To check whether Trx1 or Grx1 are involved in this redox disturbance, both redoxins were down-regulated with specific siRNA and the redox state of individual Cys residues was measured again.

3.2.2. Specific protein cysteines underwent oxidative and reductive changes upon Trx1 or Grx1 silencing depending on NOS3 overexpression

Silencing of Trx1 or Grx1 to ≈ 20% their normal levels in WT and NOS3-overexpressing HepG2 cells did result in significant redox changes of specific protein cysteines, compared with their respective controls. We had previously reported that the activities of both redoxins decreased to the same extent as Trx1 and Grx1 protein levels in their respective siRNA treated cells, excluding the induction of other active isoforms [22]. Moreover, analysis of the differential proteome of these cells in the present study did not show compensatory induction of isoforms.

A selection of target proteins with ≥ 1.5 or ≤ 0.67 fold redox changes is presented in Fig. 3A. Three groups can be distinguished in this table. i) Proteins in the upper part of the table showed sensitive cysteines which underwent an oxidative shift in WT cells, but a reductive shift in NOS3 overexpressing cells, upon silencing of either redoxin. ii) A second group in the middle part of the table shows cysteines that were more oxidized only in 4TO-NOS cells upon either redoxin silencing. iii) Finally, a third group was only sensitive towards Trx1 silencing almost exclusively in NOS3-overexpressing cells. Six proteins: Cofilin-1, 40 S ribosomal protein S5 and isoforms Gamma, Theta/delta and Beta/alpha of the 14–3-3 family of proteins, showed high sensitivity to both redoxins but their redox changes, though conspicuous, did not display clear trends and have been omitted.

These changes could be the consequence of direct interaction of either redoxin with the target proteins or could be due to indirect effects. They were almost exclusively oxidative in WT cells as one would expect from the canonical antioxidant functions of Grx1 and Trx1. However, in NOS3 overexpressing cells, the effect of silencing the redoxins, especially Trx1, also resulted in reductive changes in several protein cysteines. The reason for this apparently contradictory result could rely on the fact that NOS3 itself is sensitive to redox modification and can be activated by Trx1 and Grx1 through denitrosation and deglutathionylation [4,78]. Hence, decreasing the levels of these redoxins by specific siRNA should result in higher levels of redox modified NOS3, lower NOS3 activity and lower protein S-nitrosation levels followed by higher reduced/oxidized ratio of sensitive cysteines in target proteins. We had previously determined the level of Tyr nitration, a good indication of the degree of nitrosative/oxidative stress, in siRNA-Trx1 and siRNA-Grx1 treated WT and NOS3 overexpressing HepG2 cells [22]. Nitro-tyrosine levels were markedly higher in WT HepG2 cells but decreased to 50% in NOS3 overexpressing HepG2 cells which is a further evidence of NOS3 inactivation upon Trx1 and Grx1 down-regulation.

3.2.3. Redoxins-sensitive cysteines show specific sequence motifs

Defining sequence signatures around redox sensitive cysteines would help predict and find redox regulated target proteins. *A* search for short linear motifs in the sequences around the redox modified Cys's shown in Fig. 3A using the *motif-x* algorithm [10] produced three motifs with high enrichment score among the input set of proteins compared with the background occurrence in the whole human proteome (Fig. 3B). There is a Lys at position + 1 or + 4 in motifs 1 and 2 respectively and a threonine at + 4 in motif 3. It is well known that nucleophilic reactivity of Cys's is dependent on ionization to thiolate

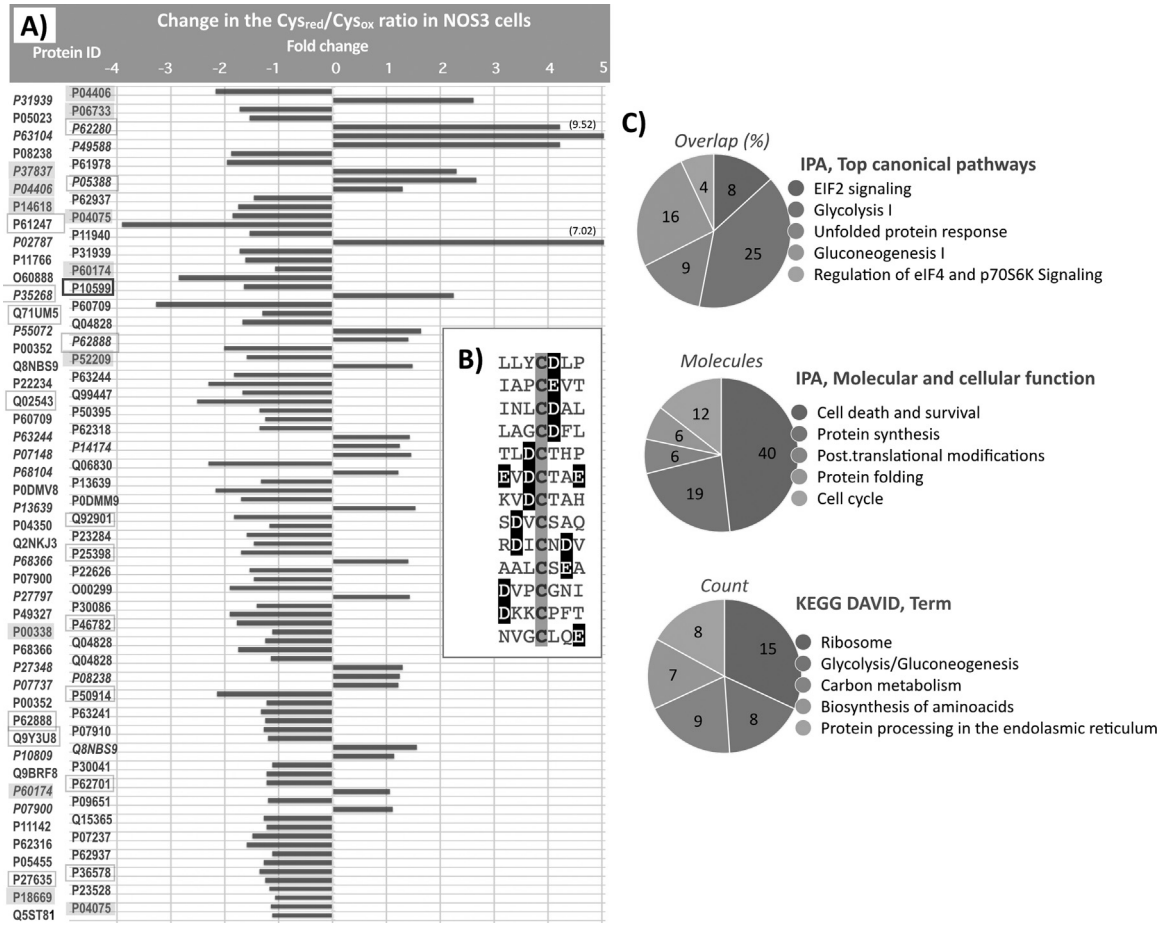

Fig. 2. NOS3 over expression alters the Reduced/Oxidized ratio of specific Cys on target proteins. A) The UniProt ID of the protein is shown in the vertical axis and the relative change in the Cys_{red}/Cys_{ox} ratio in 4TO_NOS cells is indicated in the horizontal axis as fold change relative to the ratio in control 4TO cells transformed with the empty vector. Proteins are ordered according to their statistical q score (Storey & Tibshirani) from 0.0000516 (top) to 0.0497383 (bottom). Proteins with negative values were more oxidized after NOS3 overexpression; those with positive values (IDs in *italic*) were more reduced. Two proteins showed reductive changes higher than fivefold as indicated. P10599, square boxed with thick line, is Trx1(C^{73}); ID of enzymes of Glycolysis and its branching pathways are highlighted with grey squares and ribosomal proteins are square boxed with thin line. **B)** sequence context around the cysteine residue of 13 peptides whose reduced/oxidized ratio increased ≥ 1.5 on NOS3 overexpression, showing the presence of acidic residues (white letters highlighted in black) close to the affected cysteine (grey shadowed). Protein names and Cys mapping are detailed in sheet "NOS3 Vo" of the Excel file shown in Suppl Fig. 2. **C)** Systems Biology analysis of the whole set of redox modified proteins using Ingenuity Pathway Analysis (Qiagen) and DAVID [Huang *et al. Nature Protoc. 2009;4(1):44–57*]. The five most significant terms from each analysis are shown with p values ranging from 9.18E−19 to 9.75E−04.

favored by low pKa. Computational and experimental results indicate that the surrounding charged side chains can contribute, but do not primarily control, the thiolate pKa in the Trx superfamily and other proteins with reactive Cys [69,70]. However, a search for denitrosation sites in proteins found two potential motifs with lysine at + 6 and + 7 [87] and a structural analysis of cysteine S-nitrosation sites found lysine at position + 3 and threonine at + 5 with moderate frequency [49]. The presence of a lysine residue near the target Cys is also common to human proteins S-nitrosation motifs [42]. A study that combined sequence, structure, and electrostatic approaches predicted that Thr, its hydroxyl group, and hydrogen-bonding capabilities play an important role in Cys deprotonation and reactivity [70]. Hence, our results with Lys or Thr upstream of Cys fit in with the current structural landscape of redox sensitive Cys's, where some signatures have been put forward but evidences for a strong consensus sequence motif has not yet been achieved.

Two proteins were specifically sensitive to Grx1 silencing, PGAM-1(Cys^{153}) and PRDX6(Cys^{91}). Alignment of both Cys-peptides showed a striking conservation score around the affected Cys stressing their assignment as Grx1 targets (Fig. 3C). These Cys's are positioned in a coil in the protein structure with 3.78% and 4.00% solvent accessibility, respectively, and are enriched in acidic residues around the central cysteine. They fit in the *Homo sapiens* HC05 group glutathionylation motif as catalogued at dbGSH (http://csb.cse.yzu.edu.tw/dbGSH). PRDX6 is 1-Cys peroxiredoxin with prominent features as it depends on GSH and GST-Pi for peroxidase activity and also has phospholipase A2 (PLA2) activity, which plays a role for activation of NADPH oxidase 1 and 2 (NOX1, NOX2) [17,41]. The Grx-dependent redox modified Cys at position 91 is not the canonical catalytic ("peroxidatic") cysteine that lies at position 47 of PRDX6. Cys^{91} has not been given attention so far and has been routinely substituted by Ser in the recombinant protein, supposedly to avoid unwanted thiol oxidation and "shuffling" and to facilitate handling. Further experiments have been undertaken to find out whether the Grx-specific redox sensitivity of PRDX6 Cys^{91} plays a role on any of the protein functions.

3.2.4. Part of the observed cysteine redox changes were due to direct S-nitrosation

As determined previously [21], NOS3 overexpression not only increases the levels of NO but those of other ROS as well, so reversible oxidation of Cys residues could be due to S-nitrosation or other types of oxidative modifications induced by ROS. To ascertain whether S-nitrosation was actually taking place, we have carried out the Biotin Switch Technique (BST). We have limited this analysis to siRNA-Trx1

A)

Accession	Name	Sequence	Cys residue	Ratio Cys red/Cys ox (fold change)			
				siRNA-Grx1		siRNA-Trx1	
				WT	NOS3	WT	NOS3
P08238	Heat shock protein HSP 90-beta	LVSSPCCIVTSTYGWTANMER	589-590	0,538	1,088	0,704	0,992
P11766	Alcohol dehydrogenase class-3	AGDTVIPLYIPQCGECK	97-100	0,629	1,505	0,658	1,589
P31939	Bifunctional purine biosynthesis protein PU	MSSFGDFVALSDVCDVPTAK	325	0,549	1,246	0,704	0,863
P11940	Polyadenylate-binding protein 1	ALYDTFSAFGNILSCK	128	0,673	1,635	0,797	1,366
P06733	Alpha-enolase	FGANAILGVSLAVCK	119	0,623	0,914	1,000	1,018
O75369	Filamin-B	VDIQTEDLEDGTCK	2057	0,762	1,786	0,633	1,451
P23284	Peptidyl-prolyl cis-trans isomerase B	DVIIADCGK	202	ND	0,827	ND	1,785
P23528	Cofilin 1	HELQANCYEEVK	139	0,509	1,282	0,575	1,000
P18669	Phosphoglycerate mutase 1	YADLTEDQLPSCESLK	153	0,527	1,240	1,000	1,325
Q5T6W1	Heterogeneous nuclear ribonucleoprotein	GSDFDCELR	145	0,671	1,397	0,605	0,947
P14618	Pyruvate kinase	AEGSDVANAVLDGADCIMLSGETAK	358	0,664	1,218	0,775	0,678
P30041	Peroxiredoxin-6	DINAYNCEEPTEK	91	0,444	1,201	1,000	0,974
Q15691	Microtubule-associated protein RP/EB fam	NIELICQENEGENDPVLQR	228	0,663	ND	0,674	ND
Q71UM5	40S ribosomal protein S2-like	LTEGCSFR	77	0,629	1,146	0,749	1,159
P34932	Heat shock 70 kDa protein 4	LSQECEK	270	0,637	ND	0,694	ND
P63244	Receptor of-activated protein C kinase 1	FSPNSSNPIIVSCGWDK	168	0,520	1,000	0,606	0,653
P28838	Cytosol aminopeptidase	LNLPINIIGLAPLCENMPSGK	335	0,612	ND	0,763	ND
F8WC84	55 kDa erythrocyte membrane protein	SRPEAGPLVLWCK	42	0,711	ND	0,654	ND
P00367	Glutamate dehydrogenase 1, mitochondria	IIKPCNHVLSLSFPIR	112	1,000	1,253	0,873	1,568
Q9BRF8	Serine/threonine-protein phosphatase CPP	AIPLVLVSGNHDIGNTPTAETVEEFCR	143	1,000	ND	1,000	1,723
Q9Y3U8	60S ribosomal protein L36	EVCGFAPYER	48	ND	1,233	ND	0,411
P04350	Tubulin beta-4A chain	NMMAACDPR	303	1,000	1,159	0,665	1,000
Q5ST81	Tubulin beta chain	LTTPTYGDLNHLVSATMSGVTTCLR	239	1,000	0,774	1,000	0,636
Q14974	Importin subunit beta-1	IQFNDLQSLLCATLQNVLR	585	ND	0,489	ND	0,607
P09429	High mobility group protein B1	RPPSAFFLFCSEYRPK	106	1,000	0,517	1,000	0,601
P63244	Receptor of-activated protein C kinase 1	VWNLANCK	182	ND	0,723	ND	0,656
Q9UKZ4	Teneurin-1	TIHLMHDGFICTIR	2011	ND	0,464	ND	0,294
P63241	Eukaryotic translation initiation factor 5A-1	YEDICPSTHNMDVPNIK	73	ND	0,610	ND	0,563
Q9Y678	Coatomer subunit gamma-1	ELAPAVSVLQLFCSSPK	296	ND	1,694	ND	1,830
P36776	Lon protease homolog, mitochondrial	DGPSAGCTIVTALLSLAMGRPVR	858	ND	0,841	ND	0,635
Q6P2D8	X-ray radiation resistance-associated prote	LSNPSCFASLAGL	244	ND	0,704	ND	0,654
Q9Y678	Coatomer subunit gamma-1	DSPLFDFIESCLR	258	ND	0,931	ND	1,852
P62280	40S ribosomal protein S11	DVQIGDIVTVGECRPLSK	131	0,560	1,000	1,000	1,000
P49773	Histidine triad nucleotide binding protein 1	CLAFHDISPQAPTHFLVIPK	38	1,833	ND	1,000	ND
P05388	60S acidic ribosomal protein P0	AGAIAPCEVTVPAQNTGLGPEK	119	ND	0,613	ND	1,000
P07900	Heat shock protein HSP 90-alpha	LVTSPCCIVTSTYGWTANMER	597-598	1,000	1,000	0,496	1,045
P27348	14-3-3 protein theta	YLAEVACGDDR	134	1,000	1,000	0,763	1,542
P09651	Heterogeneous nuclear ribonucleoprotein	YHTVNGHNCEVR	175	1,000	1,000	0,685	1,592
Q04828	Aldo-keto reductase family 1 member C1	LLDFCK	206	1,000	1,000	1,000	1,521
Q8NA56	Tetratricopeptide repeat protein 29	SLNLLACESLLR	230	ND	ND	ND	0,297
P07339	Cathepsin D	EGCEAIVDTGTSLMVGPVDEVR	290	ND	ND	ND	1,535
P07741	Adenine phosphoribosyltransferase	VVVVDDLLATGGTMNAACELLGR	140	ND	1,000	ND	0,550
P39023	60S ribosomal protein L3	VACIGAWHPAR	251	ND	1,000	ND	1,753
P12814	Alpha-actinin-1	MVSDINNAWGCLEQVEK	370	1,000	1,000	1,000	0,560

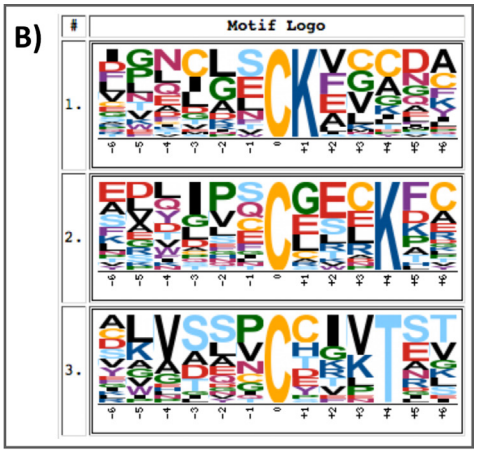

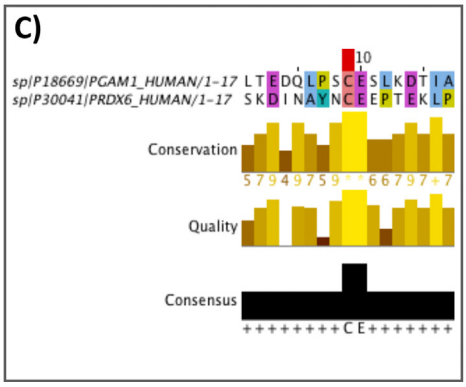

Fig. 3. Changes in the reduced/oxidized ratio of specific Cys on target proteins upon Trx1 and Grx1 silencing. A) The UniProt ID and name of the protein, the sequence of the Cys-peptide and the position of the Cys residue affected are shown together with the redox change observed expressed as fold change of the Cys_{red}/Cys_{ox} ratio relative to the non-silenced cells. Oxidative changes are colored red and reductive changes are green. Only proteins showing fold changes ≥ 1.5 or ≤ 0.66 are included. All the values are statistically significant according to their q value (Storey & Tibshirani). Cells colored yellow with a value of 1.00 represent non-significant changes; ND, peptide not detected. **B)** Putative consensus sequences of Trx1 and Grx1 related sensitive Cys-peptides; the sequences of the peptides showing significant redox changes upon Trx1 or Grx1 silencing in WT and NOS3-overexpressing HepG2 cells were subjected to Motif-X ([10]; http://motif-x.med.harvard.edu) with the following parameters: central character "C", width "13", occurrences "20", significance "0.0001", background "ipi. HUMAN.fasta"; motif scores for logos 1, 2 and 3 were 8.57, 6.30 and 4.86, respectively. **C)** Two Cys peptides specifically sensitive towards Grx1 but not Trx1 belonging to Phosphoglyceromutase-1(Cys153) and Peroxiredoxin-6(Cys91) were highly conserved as shown by pairwise alignment with a 17 residue window around the sensitive Cys, matrix EBLOSUM62, gap penalty 2; a very high conservation score was found with 2 identities (11.8%) and 6 similarities (35.3%).

treated cells, since Trx1 is well-known to display denitrosase activity.

Analysis of total biotinylated proteins by Western blotting showed clear differences between control and NOS3 overexpressing HepG2 cells as expected. When we compared Trx1 silenced cells with their control, no significant differences were detected at the level of total protein, but interestingly clear differences were found in band patterns indicating changes in S-nitrosated Cys's at the level of individual proteins: some proteins increased while others decreased upon Trx1 silencing (Fig. 4A). These results are in agreement with the finding that several proteins underwent a significant reductive shift on their key Cys's (Fig. 3).

To test individual proteins, PRDX6, PKM2, caspase-3, NOS3 and Trx1 were chosen to analyze their nitrosation state on Trx1 silencing by the BST as shown in Fig. 4B and C. All five proteins were captured with the BST, indicating that they are targets of S-nitrosation. Despite the high variability of the technique, a clear trend was observed in 4TO-NOS cells showing higher amounts of S-nitrosated PRDX6 and PKM in Trx1-silenced cells than in control cells. This trend was also observed in 4TO and in normal HepG2 cells (not shown). PRDX6 and PKM are likely substrates of Trx1 denitrosase activity, although the involved cysteines cannot be mapped with this technique and we cannot tell whether the S-nitrosated Cys are Cys^{91} or Cys^{47} in PRDX6 and Cys^{358} or another Cys in PKM. The peptide containing peroxidatic Cys^{47} of PRDX6 was not detected in any of our samples. We have previous experience on the difficulty of detecting this tryptic peptide [65], but it was detected using different technical tools in another study where Cys^{47} was actually more oxidized in sciatic nerve of old compared to young mice [56]. Since we have found that the "extra" Cys^{91} of PRDX6 is not sensitive to Trx1 but to Grx1 silencing (Fig. 3), which has no denitrosase activity, it is tempting to conclude that Cys^{47} might be target of S-nitrosation in a Trx1-dependent manner while Cys^{91} might be a Grx1-dependent target of glutathionylation. A preliminary mass spectrometric analysis of recombinant PRDX6 showed that both Cys47 and Cys91 are liable to spontaneous reversible glutahionylation (Suppl. Fig. 1). These data open the door to interesting insights into PRDX6 molecular properties and functions.

Redox sensitivity of PKM2 Cys^{358} has been reported before [2,53], however the identity of its redox reversible modification was not determined. Our data show higher S-nitrosation levels of PKM2 in Trx1 silenced cells in parallel with reversible oxidative modification of Cys^{358} suggesting PKM2 as target of Trx1 denitrosase activity. On the other hand, caspase-3, Trx1 and NOS3 itself, were S-nitrosated in NOS3 overexpressing cells, apparently to a lesser extent when Trx1 was silenced (Fig. 3C).

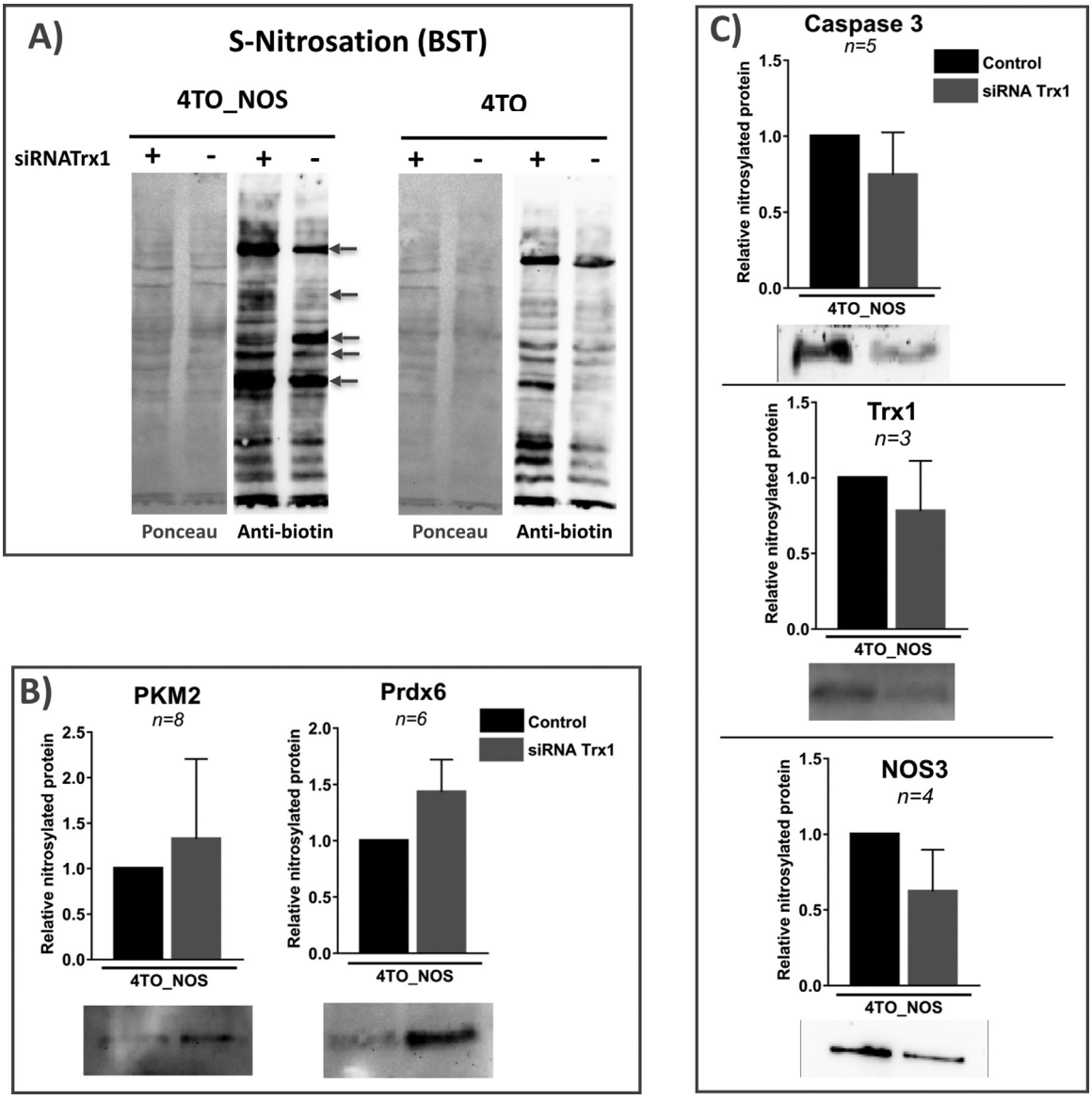

Fig. 4. Protein S-nitrosation in HepG2 cells over expressing NOS3 and treated with specific siRNA-Trx1. A) NOS3 over expressing HepG2 cells, 4TO-NOS, and control 4TO cells transformed with empty vector were silenced or not, for Trx1 and subject to BST; biotinylated proteins constituting the "S-nitrosome" were separated on SDS-PAGE, transferred to Nitrocellulose membrane and revealed with avidin-peroxidase conjugate. Membranes stained with Ponceau reagent before transfer are presented in the left panels to show the protein load. Arrows point to bands with increased or diminished intensity upon Trx1 silencing. **B)** and **C)** biotinylated proteins from 4TO-NOS HepG2 cells were captured on avidin-agarose, eluted with ß-ME, subjected to Western blot and revealed with specific antibodies to 5 selected proteins as indicated. The intensity of the bands was quantified by image analysis as described in M&M; relative abundances of each protein in the fraction of biotinylated proteins compared to non-silenced control cells are shown, together with the number of replicas and the bars showing standard deviation; trimmed images from membranes showing representative band patterns are included below each graph.

These results confirm that S-nitrosation contributes to redox changes taking place on target Cys's in HepG2 cells depending on the overexpression of NOS3 and affected by the prevailing levels of Trx1.

3.2.5. Proteins with redoxin-sensitive cysteines are abundant in Glycolysis

Clustering of redox sensitive proteins with DAVID [33,34] revealed a significant enrichment in Glycolysis in either normal or NOS3 over-expressing HepG2 cells for both redoxins, but with higher score for Grx1 silencing. Enzymes belonging to Glycolysis or its branching pathways affected by thiol redox changes upon Tx1 or Grx1 silencing or upon overexpression of NOS3 are listed in Fig. 5A and are shown in context schematically in Fig. 5B.

3.2.5.1. Glyceraldehyde-3-phosphate dehydrogenase. The peptide containing Cys^{152}/Cys^{156} of GAPDH was markedly more oxidized in NOS3 overexpressing cells. Cys^{152} is part of the active site and its oxidation renders the enzyme inactive [25,61]. We confirmed that GAPDH activity decreased in NOS3 overexpressing HepG2 cells (Fig. 5C). Silencing of Trx1 or Grx1 in normal HepG2 cells did result in diminished levels of GAPDH activity as expected, but this loss correlated with oxidation of another Cys residue, Cys^{247}, and not with the redox state of $Cys^{152/156}$, that did not change (Fig. 5A). GAPDH Cys^{247} was indeed more oxidized in Trx1 and Grx1 down-regulated WT cells, but more reduced in NOS3 overexpressing cells when Trx1 was silenced. Reversible S-thiolation of GAPDH was earlier reported [73] and since then Cys^{247} or its equivalent has been mapped and found to be S-glutathionylated, S-nitrosated and S-acetylated [24] even in plants [3], as well as a predicted target of Trx trans-nitrosation [86].

It would seem that GAPDH-C^{247} is prone to oxidative modification by nitrosation or glutathionylation under the prevailing redox cellular

A)

GLYCOLYISIS CENTERED REDOX PROTEOME CHANGES

Protein			Ratio Cys_{red}/Cys_{ox} (Fold change relative to control)				
			4TO-NOS/ 4TO	siRNA-Trx1		siRNA-Grx1	
ID	Name	Cys		WT	NOS	WT	NOS
P04075	Aldolase A (ALDOA)	339	0,54				
		178	0,87				
P06174	Triose phosphate isomerase (TPI)	255	0,94		1,29		1,42
P04406	Glyceraldehyde-3-phosphate dehydrogenase (GADH)	247	1,29	0,79	1,46	0,68	
		152/156	0,46				
P06733	Enolase (ENO)	119	0,58		0,94	0,62	0,91
P18669	Phosphoglycerate mutase (PGAM)	153	0,93			0,53	1,03
P14618	Pyruvate kinase (PKM)	358	0,58		0,68		
P00338	Lactate dehydrogenase A (LDHA)	293	0,89				
P37837	Transaldolase (TALDO)	250	2,72			0,92	
P52209	6-Phosphogluconate dehydrogenase (PGD)	170/171	0,62				
Q26210	Gln-Fructose-6-phosphate amino-transferase [isomerizing] 1 (GFAT)	434		0,79		0,82	

B)

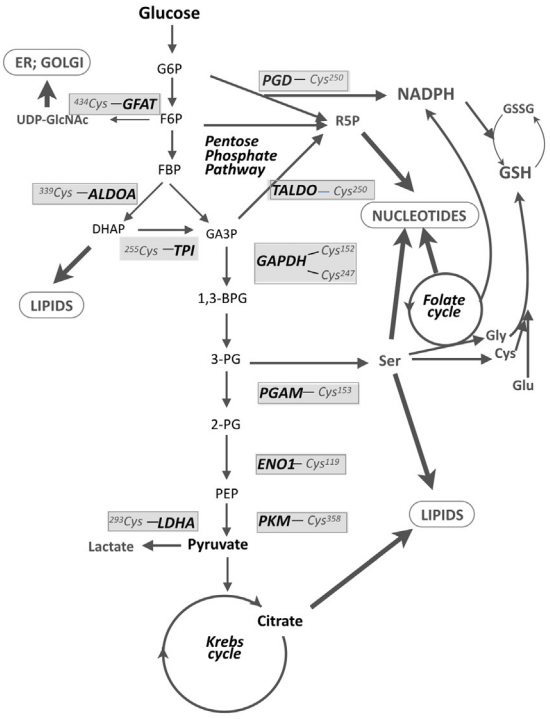

C)

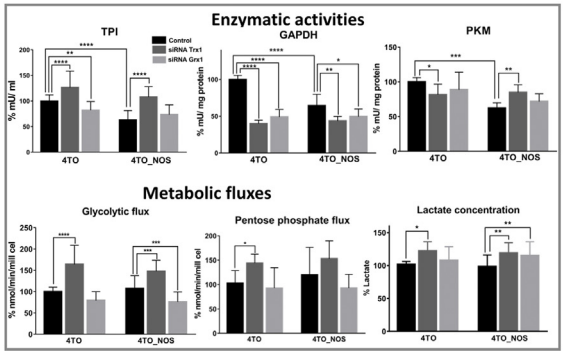

Fig. 5. Silencing Trx1 or Grx1 affects glycolytic enzymes redox state and activities and glycolytic flux. A) Enzymes of Glycolysis and related pathways undergoing significant ($q \leq 0.1$) cysteine redox changes on NOS3 overexpression and upon Trx1 or Grx1 down-regulation have been selected. The precise cysteine residues affected and the changes in the values of their reduced/oxidized cysteine ratios relative to the control (4TO-NOS *vs* 4TO; siRNA treated *vs* untreated) are shown. The values for siRNA treated 4TO-NOS cells have been weighted by subtracting the changes observed in siRNA treated 4TO control cells; **B)** Glycolysis centered metabolic network showing the main glycolytic stream and off-shooting pathways; the final destinations of metabolic fluxes are indicated with thick arrows; the enzymes with redox altered cysteines and their residue position are highlighted. **C)** Enzymatic activities of triosephosphate isomerase, glyceraldehyde-3-phosphate dehydrogenase and pyruvate kinase, Glycolysis and Pentose Phosphate Pathway fluxes and lactate concentration in siRNA Trx1 and siRNAGrx1 treated 4TO_NOS and 4TO cells are shown relative to untreated 4TO control cells. Between 4 and 9 independent experiments were done for each parameter and a Student *t*-test was calculated for statistical significance with values $p \leq 0.001$, $0.001 > p \leq 0.01$ and $0.01 > p \leq 0.05$ marked with ***, ** and *, respectively.

environment in normal HepG2 cells and to its reversal by either Trx or Grx, respectively. When this fragile equilibrium is displaced by down regulation of either redoxin, the oxidative state of Cys247 increases. However, as discussed in Section 2b, decreasing the levels of Trx1 by specific siRNA in NOS3 overexpressing cells should result in higher levels of redox modified NOS3, lower NOS3 activity and lower GAPDH-C^{247} nitrosation levels. The levels of nitro-Tyr, an indication of ROS and RNS, did actually decrease down to 50% on either redoxin silencing [22]. This would explain the reductive shift in GAPDH-C^{247}.

Besides its conventional metabolic role, a number of studies have identified the participation of GAPDH in diverse cellular functions and these oxidative changes not only affect its glycolytic function but also stimulate the participation of GAPDH in cell death [11,25]. Our findings point to Cys^{247} as a sensitive target of the antioxidant activity of Trx1 and Grx1 in WT cells with consequences on its enzymatic activity.

The rational to explain the decrease in activity of GAPDH would be that it is rewarding for the cells to slow down the glycolytic flux at this point to facilitate upstream diversion of glucose catabolism toward the Pentose Phosphate Pathway (PPP) and to increase NADPH production in this prevalent oxidative environment. However, it has yet to be demonstrated whether inactivation of GAPDH is reflected directly in slowing down of glycolytic flux. Actually, we have observed that inactivation of GAPDH in siRNA-Trx1 treated cells is paralleled by an increase in glycolytic flux (Fig. 5C). Alterations in glycolytic enzymes can regulate autophagy e.g. the moonlighting behaviour of GAPDH enables its direct interaction with mTOR [58] or translocate to the nucleus and upregulate Atg12 [11], both mechanisms being related to the activation of autophagic process. siTrx1 and siGrx1 increased caspase-3 and TUNEL in 4TO and 4TO-NOS3 cells [22] and increased the oxidative status of the heat shock 70 kDa protein 4 (HspA4) Cys^{270} (Fig. 3A), an interactor with HspA8 (heat shock cognate 71 protein), which drives chaperone-mediated autophagy [13]. Redox changes at target cysteines in GAPDH and HspA4 suggest that Trx1 and Grx1 signaling promoted a shift from autophagic survival to apoptotic pathway.

3.2.5.2. Phosphoglyceromutase-1. (PGAM1) Cys^{153} was more oxidized in WT cells when Grx1 was down-regulated. PGAM1 is commonly upregulated in human cancers and regulates anabolic biosynthesis by controlling intracellular levels of 3-phosphoglycerate (3-PG) and 2-phosphoglycerate (2-PG) to promote tumor growth [28]. Both 3-PG and 2-PG are allosteric regulators of glycolytic branching pathways: 3-PG inhibits 6-phosphogluconate dehydrogenase (6PGD) of PPP, whereas 2-PG activates phosphoglycerate dehydrogenase (PHGDH) of glycine and serine synthesis pathway. It is worth noting that activation of PGAM1 by phosphorylation at Tyr^{26}, common in human cancer cells, promotes cell proliferation and tumor growth [29]. Cys^{153} is not close to the active site but it has been noted that proteomes of Cys PTMs have localized these modifications primarily in non-catalytic regions [24]. Moreover, Cys^{153} is in the same region of the protein as Tyr^{26} and Lys^{100}. It has been demonstrated that increased levels of ROS stimulate PGAM Lys^{100} deacetylation and activity by promoting its interaction with SIRT2 [88]; its modification by oxidation could equally affect its activity or even the phosphorylation and acetylation state of Tyr^{26} and Lys^{100} located nearby.

Cellular response to oxidative stress are mediated by the HIF-1α, which is required for the upregulation of mRNAs encoding glucose

transporters and glycolytic enzymes, with the notable exception of PGAM [37], indicating a possible postranscriptional regulatory mechanism. Sensitivity of PGAM1 activity to thiol specific reagents was initially reported for the rabbit enzyme [66], but to our knowledge, this is the first time that a Grx1-dependent redox change is observed and mapped to Cys^{153} suggesting a novel form of regulation that could contribute to modulation of glycolytic flux for biosynthetic and antioxidant purposes in response to the redox environment.

3.2.5.3. Pyruvate Kinase. PKM2 (P14618-1) behaves similarly: its Cys^{358} is close to the allosteric activator fructose-1,6-*bis*phosphate (FBP) binding site and is sensitive to oxidative stress [2,53]. It has been shown that ROS-dependent inhibition of PKM2 is needed to maintain the availability of glucose-6-phosphate (G-6-P) for flux into the PPP and to sustain cell survival when endogenous ROS accumulate. Regulation of PKM2 via oxidation of Cys^{358} is critical under these conditions for optimal tumor growth [2]. Coherent with this, we show here that NOS3 overexpression oxidizes Cys^{358} accompanied by a significant decrease in activity (Fig. 5C). Cys^{358} is further oxidized when Trx1 is down-regulated, but surprisingly, PKM activity is significantly recovered to the same level as in siRNA-Trx1 treated control cells (Fig. 5C). An increase in the PKM1/PKM2 isoenzyme ratio induced by redox regulation of splicing events as reported in hepatoma cells [84] would explain this result. These data demonstrate the complexity of Trx1 involvement in maintaining the redox state of this Cys^{358} and the activity of this critical enzyme.

3.2.5.4. Enolase. Cys^{119} of Alpha-enolase is sensitive to oxidative conditions in NOS3 cells and is a target of Grx1 antioxidant activity in WT cells (Fig. 5A). This cysteine was found to be reactive toward mercury resin specific for Cys-SNO [24] and its glutathionylation in SH-SY5Y neuroblastoma cells resulted in loss of enzymatic activity [36]. Further studies will confirm the regulatory role of this Grx1 dependent redox change of α-Enolase Cys^{119}.

3.2.5.5. Triose phosphate isomerase. TPI Cys^{255} was more reduced when either Trx1 or Grx1 were silenced in NOS3 cells (Fig. 5A). TPI from several organisms has been shown to be regulated by redox changes involving glutathione at a cysteine equivalent to human Cys^{255}. The equivalent Cys in *P. falciparum* TPI, Cys^{217}, is located at the interphase of a complex formed between TPI and Trx [74], whereas *A. thaliana* TPI is inactivated by glutathionylation at Cys^{218} in a manner reverted by Grx [14]. Our results agree with these showing a significant decrease in TPI activity when Grx1 is silenced in control cells. However, silencing of either Trx1 or Grx1 in NOS3 overexpressing cells increased the activity of TPI in parallel with reduction of Cys^{255}, a likely consequence of NOS3 inactivation, as already discussed above. It is tempting to speculate that TPI Cys^{255} could act as a thiol redox switch to help divert the glycolytic flow from DHAP towards lipid synthesis as part of a metabolic response to changes in the redox environment [45].

Several enzymes from Glycolysis off-shooting pathways showed significant redox changes: Lactate dehydrogenase A (LDHA) Cys^{293} and 6-phosphogluconate dehydrogenase (PGD) $Cys^{170/171}$ were slightly more oxidized in NOS3 cells; Glutamine-Fructose-6-phosphate aminotransferase [isomerizing] 1 (GFAT) Cys^{434} was sensitive to both Trx1 and Grx1 down-regulation; and Transaldolase (TALDO) Cys^{250} was markedly more reduced in NOS3 cells

Altogether, these data show widespread redox sensitivity of key cysteines in glycolytic enzymes eventually affecting their activities. The prominent role played by Trx1 and Grx1 on these thiol redox switches could be meaningful as part of a pleiotropic redoxin reductive action as a kind of "redox regulon" [20] to coordinate an integrated response to ROS that would balance pyruvate and NADPH production and biosynthetic flux diversion (Fig. 5B). However, the precise consequences of these redoxin-dependent redox changes on metabolic fluxes cannot be predicted from the changes of individual enzymatic activities [81]. Knowledge of *Flux Control Coefficients* of each enzyme would be necessary and the fluxes through glycolysis branched pathways should also be taken into account. As a first approach we have measured glycolytic metabolic flux and metabolites levels, as described below.

3.3. Glycolytic flux and metabolite profiles were differentially affected by Trx1 and Grx1 silencing

Glycolytic and Pentose Phosphate Pathway fluxes were determined using radiolabelled glucose and measuring the formation of $[^3H]H_2O$ from [3-^{3}H]glucose during the reaction catalysed by enolase and that of $[^{14}C]CO_2$ from [1–^{14}C]glucose by 6-phophogluconate dehydrogenase, respectively. A metabolomic analysis was also undertaken. As shown in Fig. 5C, Trx1 silencing had a stimulating effect on both pathways in either NOS3 overexpressing cells and control cells, whereas Grx1 silencing had the opposite effect in all cases. These effects could be a reflection of the differential action of both redoxins on the redox state of glycolytic enzymes (see Fig. 5A).

3.3.1. Grx1 silencing slows down Glycolysis and stimulates lipogenesis

The relationships between cysteine redox state, enzymatic activities and metabolic fluxes are not straightforward, the metabolic profiles in siRNA-Grx1 treated cells were coherent with lower glycolytic flux showing increased levels of extracellular and intracellular glucose (Fig. 6A). Sedoheptulose-7-phosphate (Su7P) accumulated in WT and NOS3 overexpressing HepG2 cells treated with siRNA-Grx1 (Fig. 6B). This was accompanied by increased levels of several polyols including arabitol, xylitol, ribitol, mannitol and sorbitol, indicative of transaldolase (TALDO) malfunctioning [76], and decreased levels of ribose. These metabolic changes indicate slowing down of glucose processing through the non-oxidative part of PPP as a consequence of Grx1 silencing. Redox changes detected in TALDO-Cys^{250}, 6-phosphogluconate dehydrogenase (PGD) $Cys1^{70/171}$ and TPI-Cys^{255} could be involved in the underlying regulatory mechanisms.

Another effect of Grx1 silencing was an increase in 3-phosphoglycerate (3PG) and lower levels of pyruvate (Fig. 6C) coincident with PGAM-Cys^{153} oxidation and likely deviation of 3PG toward serine pathway. Moreover, unchanged or increased levels of citrate and lower levels of α-ketoglutarate and fumarate (Fig. 6D), might indicate slowing down of Krebs cycle but deviation of citrate to fatty acid biosynthesis. Accordingly, elevated levels of acyl-carnitine (Fig. 6H) and *de novo* synthesis of phospholipids, was evidenced in siRNA-Grx1 treated cells, represented by high levels of phosphatidylcholine and the family of 2-arachidonoyl phospholipids with the exception of phosphatidylserine (Figs. 6L and 6N). The increase in 2-arachidonoyl phospholipids runs parallel with oxidation of PRDX6 Cys^{91} and it is worth noting the specificity of cytosolic Ca^{2+}-independent PLA2 activity for *sn*-2-arachidonic acid glycerophospholipids [63], a precursor of eicosanoids, which represent a class of lipid mediators. Moreover, arachidonic acid has been shown to mediate the known proliferative action of PRDX6 [72]. These changes speak of active membrane remodeling and/or lipid signaling events in Grx1 down-regulated cells.

Levels of several intermediary metabolites of purine pathway were markedly elevated in Grx1 silenced cells with the exception of IMP but including S-adenosylmethionine (SAM) (Fig. 6G). Elevated levels of SAM should indicate intensification of the methionine/folate pathway connected to glutathione synthesis and supplier of NADPH as an alternative to PPP (Fig. 5B). The synthesis of glutathione was actually exacerbated as indicated by increased levels of gamma-glutamylcysteine and cysteinylglycine (Fig. 6F).

3.3.2. Trx1 silencing induces membrane remodeling

There were similarities and differences between the effects of Grx1 and Trx1 silencing in metabolites' levels. Increased glutathione metabolism (Fig. 6F) and a marked decrease in 3-hydroxy-3-methylglutarate (Fig. 6M) of mevalonate pathway are among the coincidences, but the

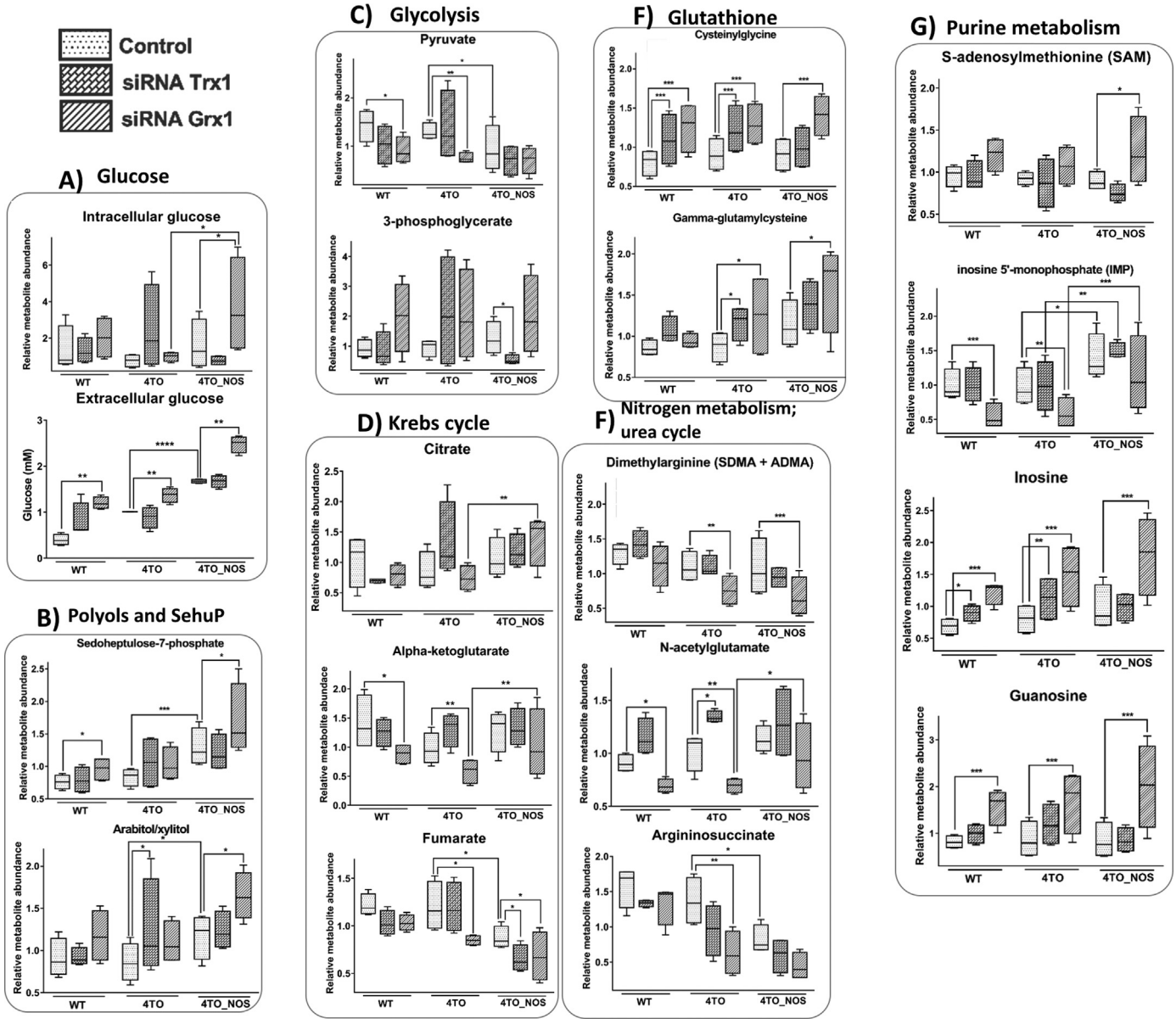

Fig. 6. Metabolites concentrations in normal and NOS3 overexpressing HepG2 under Trx1 and Grx1 down-regulation. A metabolomics analysis was performed in normal (WT), 4TO and 4TO_NOS cells treated with siRNA-Trx1, siRNA-Grx1 or control siRNA-nonTarget as described in Materials & Methods. A selection of metabolites representing the most conspicuous changing trends when cells are treated with siRNA-Trx1 or siRNA-Grx1 is shown. The results presented in this figure are part of a larger metabolic study. Extracellular glucose concentration was determined in culture media by a standard method independently of the metabolomic analysis.

levels of gamma-glutamylaminoacids is higher in siRNA-Grx1 (see Suppl. File 3) and siRNA-Trx1 did not affect Su7P and glucose levels (Fig. 6B). Trx silencing elicited trending and significant increases in dipeptides (see Suppl. File 3) that may reflect increased proteasome-mediated elimination of oxidized proteins in the setting of oxidative stress. Increases in protein degradation could suggest Keap1-Nrf2 signaling and increased autophagy. Notably, many of these changes were not observed in NOS3 overexpressing 4TO_NOS cells.

Trx1 silencing also showed signs of lipid remodeling but differed from Grx1 in promoting a trend of increasing sphingomyelins and ceramides (Figs. 6I and 6J). Ceramide is involved in apoptotic processes and in the formation of membrane raft redox signaling platforms (MRRSP) that participate in the assembly and activation of NOX complexes [62]. These changes are consistent with the pro-apoptotic effect of Trx and Grx silencing in these cells as we had already reported [22]. The sensitivity of sphingomyelinases to redox changes is a key to the cross-talk between sphingolipids and redox signaling through the regulation of NADPH oxidase, mitochondrial integrity, NOS, and antioxidant enzymes [7]. The trend of sphingomyelins' pool increase on Trx1 silencing could have an influence on mitochondrial lipid composition and integrity. However, cardiolipin, a typical and prominently functional mitochondrial phospholipid, was not detected. Hence, involvement of mitochondria cannot be excluded and is worth of further attention.

4. Conclusions

In the cell there is a delicate balance between effective redox signaling mechanisms and potentially damaging oxidative damage. Oxidative/nitrosative induced PTMs are critical for the accumulation of redox modified proteins, induction of autophagy, and further cellular apoptosis in unsolved pathophysiological intracellular responses while

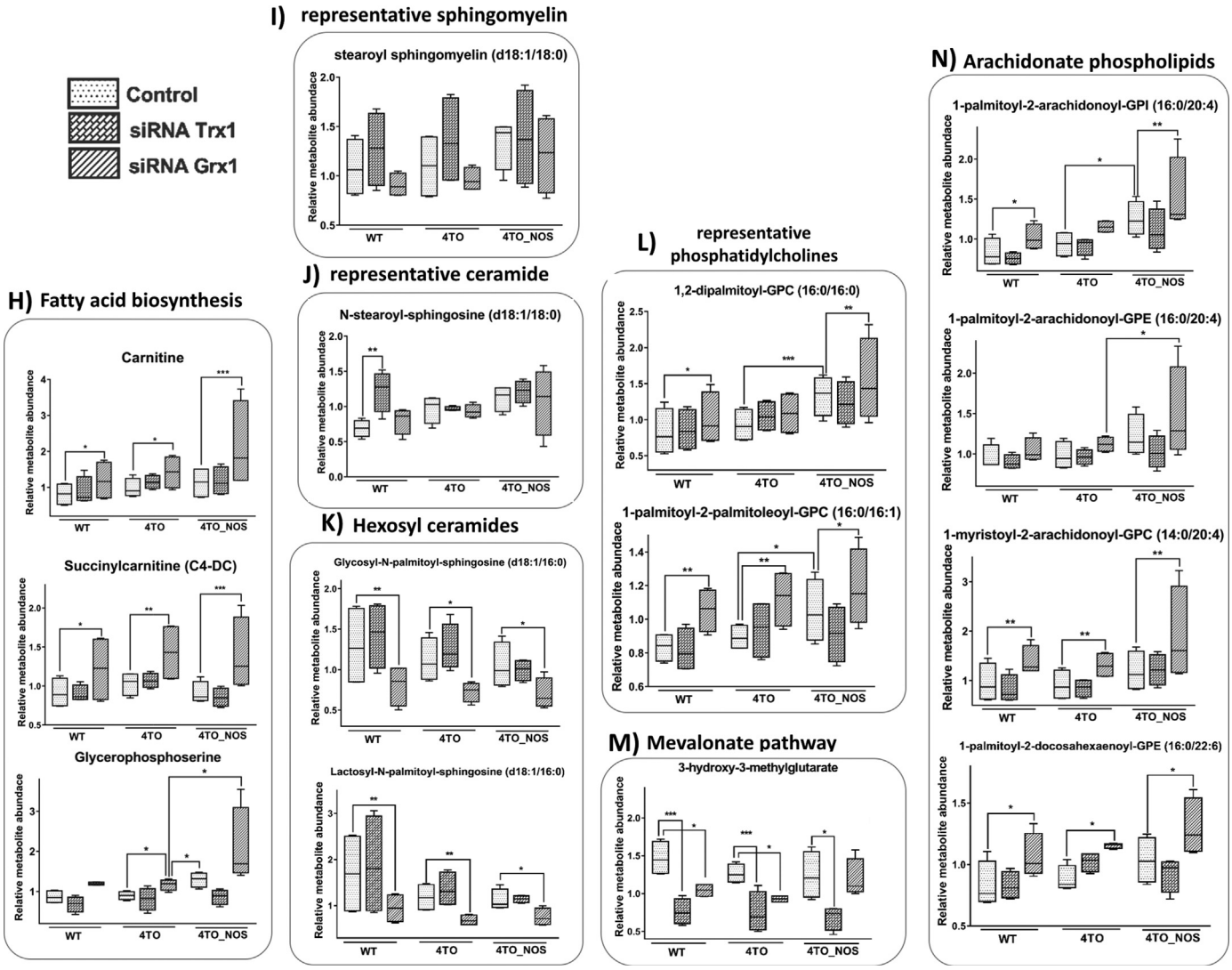

Fig. 6. (*continued*)

redox signaling through the transient oxidation/reduction of key Cys residues in regulatory proteins plays a role in many of the hallmarks of cancer [31].

The data presented herein show that Trx and/or Grx are involved in redox modifications of targeted cysteines of several glycolytic enzymes affecting their activity, although changes in the activity of one single enzyme cannot be extrapolated to equivalent changes in overall metabolic flux. These changes are part of a widespread adaptive mechanism aimed at redistributing metabolic fluxes between Glycolysis and its off-shooting pathways to respond to subtle changes in the cellular redox environment. Trx and Grx share a number of protein Cys redox targets but down regulation of either redoxin has markedly different metabolic outcomes: silencing of Trx1 stimulates glycolytic flux while silencing of Grx1 decelerates it.

Besides its canonical antioxidant action, Trx1 also contributes to oxidative modifications of protein thiols, likely by activation of NOS3, reflecting the delicate sensitivity of redox equilibrium to changes in any of the elements involved and the difficulty of forecasting metabolic responses to redox environmental changes.

A correlation can be put forward between the reversible oxidation of Cys91 of PRDX6 upon Grx1 silencing that is accompanied by a significative increase of *sn*-2-arachidonoyl containing phospholipids and Cys91 sensitivity to glutathionylation, considering the well-known deglutathionylase activity of Grx.

To our knowledge, this is the first demonstration of a role for Grx1 and Trx1 in the crosstalk between lipids metabolism and redox signaling. Further and deeper insights into the underlying mechanisms, *i.e.* possible involvement of PRDX6 and Nrf2 signaling [40], CD95 ligand or TNFα induced activation of sphingomyelinases and ceramide induced MRRSP activation of NOX [18], etc., are expected to be discovered with ongoing focused experiments.

Acknowledgements

This research has been financed by grants from the Spanish Ministry of Economy and Competitiveness (BFU2016-80006-P), the Andalusian Government (Consejería de Economía, Innovación, Ciencia y Empleo, BIO-0216 and CTS-6264 and Consejería de Igualdad, Salud y Políticas Sociales, PI-00025-2013 and PI-0198-2016), Institute of Health Carlos III, Spain (PI13/00021, PI16/00090, CIBEREHD and CIBERNED) co-financed by European Development Regional Fund, Europe. We are indebted to Beatriz Carmona (EJ17-BIO216, Programa de Empleo Joven, FEDER/Junta de Andalucía) for her excellent technical assistance in the Biochemistry and Molecular Biology lab.

Appendix A. Supplementary material

Supplementary data associated with this article can be found in the

online version at doi:10.1016/j.redox.2018.11.007.

References

[1] W.K. Alderton, C.E. Cooper, R.G. Knowles, Nitric oxide synthases: structure, function and inhibition, Biochem J 357 (2001) 593–615.

[2] D. Anastasiou, G. Poulogiannis, J.M. Asara, M.B. Boxer, J.-K. Jiang, M. Shen, G. Bellinger, A.T. Sasaki, J.W. Locasale, D.S. Auld, C.J. Thomas, M.G. Vander Heiden, L.C. Cantley, Inhibition of pyruvate kinase M2 by reactive oxygen species contributes to cellular antioxidant responses, Science 334 (2011) 1278–1283.

[3] M. Bedhomme, M. Adamo, C.H. Marchand, J. Couturier, N. Rouhier, S.D. Lemaire, M. Zaffagnini, P. Trost, Glutathionylation of cytosolic glyceraldehyde-3-phosphate dehydrogenase from the model plant Arabidopsis thaliana is reversed by both glutaredoxins and thioredoxins in vitro, Biochem J 445 (2012) 337–347.

[4] M. Benhar, Nitric oxide and the thioredoxin system: a complex interplay in redox regulation, Biochim. Biophys. Acta 1850 (2015) 2476–2484.

[5] M. Benhar, M.T. Forrester, D.T. Hess, J.S. Stamler, Regulated Protein Denitrosylation by Cytosolic and Mitochondrial Thioredoxins, Science 320 (2008) 1050–1054.

[6] M. Benhar, J.W. Thompson, M.A. Moseley, J.S. Stamler, Identification of S-nitrosylated targets of thioredoxin using a quantitative proteomic approach, Biochemistry 49 (2010) 6963–6969.

[7] O.M. Bhat, X. Yuan, G. Li, R. Lee, P.-L. Li, Sphingolipids and Redox Signaling in Renal Regulation and Chronic Kidney Diseases, *Antioxid Redox Signal*, ars 2017 (2018) 7129–7154.

[8] B.B. Buchanan, Y. Balmer, Redox regulation: a broadening horizon, Annu Rev Plant Biol 56 (2005) 187–220.

[9] C.-A. Chen, F. De Pascali, A. Basye, C. Hemann, J.L. Zweier, Redox modulation of endothelial nitric oxide synthase by glutaredoxin-1 through reversible oxidative post-translational modification, Biochemistry 52 (2013) 6712–6723.

[10] M.F. Chou, D. Schwartz, Biological sequence motif discovery using motif-x, Curr Protoc Bioinformatics (2011) 15–24 Chapter 13, Unit13.

[11] A. Colell, D.R. Green, J.-E. Ricci, Novel roles for GAPDH in cell death and carcinogenesis, Cell Death Differ. 16 (2009) 1573–1581.

[12] J. Cox, M. Mann, MaxQuant enables high peptide identification rates, individualized p.p.b.-range mass accuracies and proteome-wide protein quantification, Nat Biotechnol 26 (2008) 1367–1372.

[13] M. Dodson, V. Darley-Usmar, J. Zhang, Cellular metabolic and autophagic pathways: traffic control by redox signaling, Free Radic Biol Med 63 (2013) 207–221.

[14] S. Dumont, N.V. Bykova, G. Pelletier, S. Dorion, J. Rivoal, Cytosolic Triosephosphate Isomerase from Arabidopsis thaliana Is Reversibly Modified by Glutathione on Cysteines 127 and 218, Front Plant Sci 7 (2016) 1942.

[15] P.A. Erwin, A.J. Lin, D.E. Golan, T. Michel, Receptor-regulated dynamic S-nitrosylation of endothelial nitric-oxide synthase in vascular endothelial cells, J Biol Chem 280 (2005) 19888–19894.

[16] S. Fielek, H.W. Mohrenweiser, Erythrocyte Enzyme Deficiencies Assessed with a Miniature Centrifugal Analyzer, Clin. Chem. 25 (1979) 384–388.

[17] A.B. Fisher, Peroxiredoxin 6 in the repair of peroxidized cell membranes and cell signaling, Arch Biochem Biophys 617 (2017) 68–83.

[18] C.R. Gault, L.M. Obeid, Y.A. Hannun, An Overview of Sphingolipid Metabolism: From Synthesis to Breakdown, Adv. Exp. Med. Biol. 688 (2010) 1–23.

[19] Y.-M. Go, D.P. Jones, Thiol/disulfide redox states in signaling and sensing, Critical Reviews in Biochemistry and Molecular Biology (2013) 1–19.

[20] Y.M. Go, D.P. Jones, The Redox Proteome, Journal of Biological Chemistry (2013).

[21] R. González, G. Ferrín, P. Aguilar-Melero, I. Ranchal, C.I. Linares, R.I. Bello, M. la Mata de, V. Gogvadze, J.A. Bárcena, J.M. Alamo, S. Orrenius, F.J. Padillo, B. Zhivotovsky, J. Muntané, Targeting hepatoma using nitric oxide donor strategies, Antioxid Redox Signal 18 (2013) 491–506.

[22] R. González, M.J. López-Grueso, J. Muntané, J.A. Bárcena, C.A. Padilla, Redox regulation of metabolic and signaling pathways by thioredoxin and glutaredoxin in NOS-3 overexpressing hepatoblastoma cells, *Redox Biology* 6 (2015) 122–134.

[23] R. González, F.J. Molina-Ruiz, J.A. Bárcena, C.A. Padilla, J. Muntané, Regulation of Cell Survival, Apoptosis, and Epithelial-to-Mesenchymal Transition by Nitric Oxide-Dependent Post-Translational Modifications, Antioxid Redox Signal 29 (2018) 1312–1332.

[24] N.S. Gould, P. Evans, P. Martínez-Acedo, S.M. Marino, V.N. Gladyshev, K.S. Carroll, H. Ischiropoulos, Site-Specific Proteomic Mapping Identifies Selectively Modified Regulatory Cysteine Residues in Functionally Distinct Protein Networks, Chemistry & Biology 22 (2015) 965–975.

[25] M.R. Hara, N. Agrawal, S.F. Kim, M.B. Cascio, M. Fujimuro, Y. Ozeki, M. Takahashi, J.H. Cheah, S.K. Tankou, L.D. Hester, C.D. Ferris, S.D. Hayward, S.H. Snyder, A. Sawa, S-nitrosylated GAPDH initiates apoptotic cell death by nuclear translocation following Siah1 binding, Nat. Cell Biol. 7 (2005) 665–674.

[26] S.I. Hashemy, A. Holmgren, Regulation of the catalytic activity and structure of human thioredoxin 1 via oxidation and S-nitrosylation of cysteine residues, J Biol Chem 283 (2008) 21890–21898.

[27] J.M. Held, S.R. Danielson, J.B. Behring, C. Atsriku, D.J. Britton, R.L. Puckett, B. Schilling, J. Campisi, C.C. Benz, B.W. Gibson, Targeted quantitation of site-specific cysteine oxidation in endogenous proteins using a differential alkylation and multiple reaction monitoring mass spectrometry approach, Molecular & Cellular Proteomics 9 (2010) 1400–1410.

[28] T. Hitosugi, L. Zhou, S. Elf, J. Fan, H.-B. Kang, J.H. Seo, C. Shan, Q. Dai, L. Zhang, J. Xie, T.-L. Gu, P. Jin, M. Alečković, G. LeRoy, Y. Kang, J.A. Sudderth, R.J. DeBerardinis, C.-H. Luan, G.Z. Chen, S. Muller, D.M. Shin, T.K. Owonikoko, S. Lonial, M.L. Arellano, H.J. Khoury, F.R. Khuri, B.H. Lee, K. Ye, T.J. Boggon, S. Kang, C. He, J. Chen, Phosphoglycerate mutase 1 coordinates glycolysis and biosynthesis to promote tumor growth, Cancer Cell 22 (2012) 585–600.

[29] T. Hitosugi, L. Zhou, J. Fan, S. Elf, L. Zhang, J. Xie, Y. Wang, T.-L. Gu, M. Alečković, G. LeRoy, Y. Kang, H.-B. Kang, J.H. Seo, C. Shan, P. Jin, W. Gong, S. Lonial, M.L. Arellano, H.J. Khoury, G.Z. Chen, D.M. Shin, F.R. Khuri, T.J. Boggon, S. Kang, C. He, J. Chen, Tyr26 phosphorylation of PGAM1 provides a metabolic advantage to tumours by stabilizing the active conformation, Nat Commun 4 (2013) 1790.

[30] A. Holmgren, C. Johansson, C. Berndt, M.E. Lönn, C. Hudemann, C.H. Lillig, Thiol redox control via thioredoxin and glutaredoxin systems, Biochem Soc Trans 33 (2005) 1375–1377.

[31] M. Hornsveld, T.B. Dansen, The Hallmarks of Cancer from a Redox Perspective, Antioxid Redox Signal 25 (2016) 300–325.

[32] W. Hu, S. Tedesco, B. McDonagh, J.A. Bárcena, C. Keane, D. Sheehan, Selection of thiol- and disulfide-containing proteins of Escherichia coli on activated thiol-Sepharose, Analytical Biochemistry 398 (2010) 245–253.

[33] D.W. Huang, B.T. Sherman, R.A. Lempicki, Bioinformatics enrichment tools: paths toward the comprehensive functional analysis of large gene lists, Nucleic Acids Res 37 (2009) 1–13.

[34] D.W. Huang, B.T. Sherman, R.A. Lempicki, Systematic and integrative analysis of large gene lists using DAVID bioinformatics resources, Nat Protoc 4 (2009) 44–57.

[35] C. Inadomi, H. Murata, Y. Ihara, S. Goto, Y. Urata, J. Yodoi, T. Kondo, K. Sumikawa, Overexpression of glutaredoxin protects cardiomyocytes against nitric oxide-induced apoptosis with suppressing the S-nitrosylation of proteins and nuclear translocation of GAPDH, Biochemical and Biophysical Research Communications (2012) 1–6.

[36] T. Ishii, K. Uchida, Induction of reversible cysteine-targeted protein oxidation by an endogenous electrophile 15-deoxy-delta12,14-prostaglandin J2, Chem Res Toxicol 17 (2004) 1313–1322.

[37] N.V. Iyer, L.E. Kotch, F. Agani, S.W. Leung, E. Laughner, R.H. Wenger, M. Gassmann, J.D. Gearhart, A.M. Lawler, A.Y. Yu, G.L. Semenza, Cellular and developmental control of O2 homeostasis by hypoxia-inducible factor 1 alpha, Genes Dev. 12 (1998) 149–162.

[38] P.A. Karplus, L.B. Poole, Cysteine-based redox switches in enzymes, Antioxid Redox Signal 14 (2011) 1065–1077.

[39] P. Klatt, S. Lamas, Regulation of protein function by S-glutathiolation in response to oxidative and nitrosative stress, FEBS J 267 (2000) 4928–4944.

[40] O. Kuda, M. Brezinova, J. Silhavy, V. Landa, V. Zidek, C. Dodia, F. Kreuchwig, M. Vrbacky, L. Balas, T. Durand, N. Hübner, A.B. Fisher, J. Kopecky, M. Pravenec, Nrf2-mediated Antioxidant Defense and Peroxiredoxin 6 are Linked to Biosynthesis of Palmitic Acid Ester of 9-Hydroxystearic Acid, Diabetes. (2018).

[41] J. Kwon, A. Wang, D.J. Burke, H.E. Boudreau, K.J. Lekstrom, A. Korzeniowska, R. Sugamata, Y.-S. Kim, L. Yi, I. Ersoy, S. Jaeger, K. Palaniappan, D.R. Ambruso, S.H. Jackson, T.L. Leto, Peroxiredoxin 6 (Prdx6) supports NADPHoxidase1 (Nox1)-based superoxide generation and cell migration, Free Radic Biol Med. (2016).

[42] T.-Y. Lee, Y.-J. Chen, T.-C. Lu, H.-D. Huang, Y.-J. Chen, SNOSite: exploiting maximal dependence decomposition to identify cysteine S-nitrosylation with substrate site specificity, PLoS ONE 6 (2011) e21849.

[43] L.I. Leichert, U. Jakob, Quantifying changes in the thiol redox proteome upon oxidative stress in vivo, Proc Natl Acad Sci USA 105 (2008) 8197–8202.

[44] C.-Q. Li, G.N. Wogan, Nitric oxide as a modulator of apoptosis, Cancer Lett 226 (2005) 1–15.

[45] P.-L. Li, E. Gulbins, Bioactive Lipids and Redox Signaling: Molecular Mechanism and Disease Pathogenesis, Antioxid Redox Signal. (2018).

[46] M. Lindahl, A. Mata-Cabana, T. Kieselbach, The disulfide proteome and other reactive cysteine proteomes: analysis and functional significance, Antioxid Redox Signal 14 (2011) 2581–2642.

[47] L. Liu, A. Hausladen, M. Zeng, L. Que, J. Heitman, J.S. Stamler, A metabolic enzyme for S-nitrosothiol conserved from bacteria to humans, Nature 410 (2001) 490–494.

[48] B. MacLean, D.M. Tomazela, N. Shulman, M. Chambers, G.L. Finney, B. Frewen, R. Kern, D.L. Tabb, D.C. Liebler, M.J. MacCoss, Skyline: an open source document editor for creating and analyzing targeted proteomics experiments, Bioinformatics 26 (2010) 966–968.

[49] S.M. Marino, V.N. Gladyshev, Structural analysis of cysteine S-nitrosylation: a modified acid-based motif and the emerging role of trans-nitrosylation, J Mol Biol 395 (2010) 844–859.

[50] P. Martínez-Acedo, E. Núñez, F.J.S. Gómez, M. Moreno, E. Ramos, A. Izquierdo-Álvarez, E. Miro-Casas, R. Mesa, P. Rodriguez, A. Martínez-Ruiz, D.G. Dorado, S. Lamas, J. Vázquez, A novel strategy for global analysis of the dynamic thiol redox proteome, Mol Cell Proteomics 11 (2012) 800–813.

[51] A. Martínez-Ruiz, S. Lamas, Detection and proteomic identification of S-nitrosylated proteins in endothelial cells, Arch Biochem Biophys 423 (2004) 192–199.

[52] A. Martínez-Ruiz, I.M. Araújo, A. Izquierdo-Álvarez, P. Hernansanz-Agustín, S. Lamas, J.M. Serrador, Specificity in S-nitrosylation: a short-range mechanism for NO signaling? Antioxid Redox Signal 19 (2013) 1220–1235.

[53] B. McDonagh, S. Ogueta, G. Lasarte, C.A. Padilla, J.A. Bárcena, Shotgun redox proteomics identifies specifically modified cysteines in key metabolic enzymes under oxidative stress in Saccharomyces cerevisiae, J Proteomics 72 (2009) 677–689.

[54] B. McDonagh, J.R. Pedrajas, C.A. Padilla, J.A. Bárcena, Thiol redox sensitivity of two key enzymes of heme biosynthesis and pentose phosphate pathways: uroporphyrinogen decarboxylase and transketolase, Oxid Med Cell Longev 2013 (2013) 932472–13.

[55] B. McDonagh, G.K. Sakellariou, N.T. Smith, P. Brownridge, M.J. Jackson, Differential cysteine labeling and global label-free proteomics reveals an altered metabolic state in skeletal muscle aging, J Proteome Res 13 (2014) 5008–5021.

[56] B. McDonagh, S.M. Scullion, A. Vasilaki, N. Pollock, A. McArdle, M.J. Jackson,

Ageing-induced changes in the redox status of peripheral motor nerves imply an effect on redox signalling rather than oxidative damage, Free Radic Biol Med 94 (2016) 27–35.
[57] C.M. Metallo, M.G. Vander Heiden, Understanding metabolic regulation and its influence on cell physiology, Molecular Cell 49 (2013) 388–398.
[58] N.L. Mi, H.H. Sang, J. Kim, A. Koh, S.L. Chang, H.K. Jung, H. Jeon, D.-H. Kim, P.-G. Suh, H.R. Sung, Glycolytic flux signals to mTOR through glyceraldehyde-3-phosphate dehydrogenase-mediated regulation of Rheb, Mol Cell Biol 29 (2009) 3991–4001.
[59] J.J. Mieyal, M.M. Gallogly, S. Qanungo, E.A. Sabens, M.D. Shelton, Molecular mechanisms and clinical implications of reversible protein S-glutathionylation, Antioxid Redox Signal 10 (2008) 1941–1988.
[60] D.A. Mitchell, M.A. Marletta, Thioredoxin catalyzes the S-nitrosation of the caspase-3 active site cysteine, Nature Chemical Biology 1 (2005) 154–158.
[61] S. Mohr, J.S. Stamler, B. Brüne, Posttranslational modification of glyceraldehyde-3-phosphate dehydrogenase by S-nitrosylation and subsequent NADH attachment, J Biol Chem 271 (1996) 4209–4214.
[62] M.J. Morgan, Y.-S. Kim, Z. Liu, Lipid rafts and oxidative stress-induced cell death, Antioxid Redox Signal 9 (2007) 1471–1483.
[63] M. Murakami, I. Kudo, Phospholipase A2, J. Biochem. 131 (2002) 285–292.
[64] J.M. Patel, J. Zhang, E.R. Block, Nitric oxide-induced inhibition of lung endothelial cell nitric oxide synthase via interaction with allosteric thiols: role of thioredoxin in regulation of catalytic activity, Am. J. Respir. Cell Mol. Biol. 15 (1996) 410–419.
[65] J.R. Pedrajas, B. McDonagh, F. Hernández-Torres, A. Miranda-Vizuete, R. González-Ojeda, E. Martínez-Galisteo, C.A. Padilla, J.A. Bárcena, Glutathione Is the Resolving Thiol for Thioredoxin Peroxidase Activity of 1-Cys Peroxiredoxin Without Being Consumed During the Catalytic Cycle, Antioxid Redox Signal 24 (2016) 115–128.
[66] M.O. Prehu, C. Prehu, M.C. Calvin, R. Rosa, Rabbit M type phosphoglyceromutase: comparative effects of two thiol reagents antibody reaction and hybridization studies, Comp. Biochem. Physiol., B 89 (1988) 257–262.
[67] K. Ravi, L.A. Brennan, S. Levic, P.A. Ross, S.M. Black, S-nitrosylation of endothelial nitric oxide synthase is associated with monomerization and decreased enzyme activity, Proc Natl Acad Sci USA 101 (2004) 2619–2624.
[68] R. Requejo-Aguilar, I. Lopez-Fabuel, D. Jimenez-Blasco, E. Fernandez, A. Almeida, J.P. Bolaños, DJ1 represses glycolysis and cell proliferation by transcriptionally up-regulating Pink1, Biochem J 467 (2015) 303–310.
[69] G. Roos, N. Foloppe, J. Messens, Understanding the pK(a) of redox cysteines: the key role of hydrogen bonding, Antioxid Redox Signal 18 (2013) 94–127.
[70] F.R. Salsbury, S.T. Knutson, L.B. Poole, J.S. Fetrow, Functional site profiling and electrostatic analysis of cysteines modifiable to cysteine sulfenic acid, Protein Sci 17 (2008) 299–312.
[71] B. Schilling, M.J. Rardin, B.X. MacLean, A.M. Zawadzka, B.E. Frewen, M.P. Cusack, D.J. Sorensen, M.S. Bereman, E. Jing, C.C. Wu, E. Verdin, C.R. Kahn, M.J. MacCoss, B.W. Gibson, Platform-independent and Label-free Quantitation of Proteomic Data Using MS1 Extracted Ion Chromatograms in Skyline: APPLICATION TO PROTEIN ACETYLATION AND PHOSPHORYLATION, Molecular & Cellular Proteomics 11 (2012) 202–214.
[72] A. Schmitt, W. Schmitz, A. Hufnagel, M. Schartl, S. Meierjohann, Peroxiredoxin 6 triggers melanoma cell growth by increasing arachidonic acid-dependent lipid signalling, Biochem J 471 (2015) 267–279.
[73] I. Schuppe-Koistinen, P. Moldéus, T. Bergman, I.A. Cotgreave, S-thiolation of human endothelial cell glyceraldehyde-3-phosphate dehydrogenase after hydrogen peroxide treatment, Eur J Biochem 221 (1994) 1033–1037.
[74] H.M.S. Shahul, S.P. Sarma, The structure of the thioredoxin-triosephosphate isomerase complex provides insights into the reversible glutathione-mediated regulation of triosephosphate isomerase, Biochemistry 51 (2012) 533–544.
[75] M.D. Shelton, P.B. Chock, J.J. Mieyal, Glutaredoxin: role in reversible protein s-glutathionylation and regulation of redox signal transduction and protein translocation, Antioxid Redox Signal 7 (2005) 348–366.
[76] A. Stincone, A. Prigione, T. Cramer, M.M.C. Wamelink, K. Campbell, E. Cheung, V. Olin-Sandoval, N.-M. Grüning, A. Krüger, M. Tauqeer Alam, M.A. Keller, M. Breitenbach, K.M. Brindle, J.D. Rabinowitz, M. Ralser, The return of metabolism: biochemistry and physiology of the pentose phosphate pathway, Biol Rev 90 (2014) 927–963.
[77] J.D. Storey, R. Tibshirani, Statistical significance for genomewide studies, Proceedings of the National Academy of Sciences 100 (2003) 9440–9445.
[78] J. Subramani, V. Kundumani-Sridharan, R.H.P. Hilgers, C. Owens, K.C. Das, Thioredoxin Uses a GSH-independent Route to Deglutathionylate Endothelial Nitric-oxide Synthase and Protect against Myocardial Infarction, J Biol Chem 291 (2016) 23374–23389.
[79] L.B. Sullivan, D.Y. Gui, M.G.V. Heiden, Altered metabolite levels in cancer: implications for tumour biology and cancer therapy, Nat. Rev. Cancer 16 (2016) 680–693.
[80] D.A. Tennant, R.V. Durán, E. Gottlieb, Targeting metabolic transformation for cancer therapy, Nat. Rev. Cancer 10 (2010) 267–277.
[81] B. Teusink, J. Passarge, C.A. Reijenga, E. Esgalhado, C.C. van der Weijden, M. Schepper, M.C. Walsh, B.M. Bakker, K. van Dam, H.V. Westerhoff, J.L. Snoep, Can yeast glycolysis be understood in terms of in vitro kinetics of the constituent enzymes? Testing biochemistry, Eur J Biochem 267 (2000) 5313–5329.
[82] S. Tyanova, T. Temu, J. Cox, The MaxQuant computational platform for mass spectrometry–based shotgun proteomics, Nat Protoc 11 (2016) 2301–2319.
[83] M.G. Vander Heiden, L.C. Cantley, C.B. Thompson, Understanding the Warburg effect: the metabolic requirements of cell proliferation, Science 324 (2009) 1029–1033.
[84] L. Wei, Y. Dai, Y. Zhou, Z. He, J. Yao, L. Zhao, Q. Guo, L. Yang, Oroxylin A activates PKM1/HNF4 alpha to induce hepatoma differentiation and block cancer progression, Cell Death and Disease 8 (2017) e2944.
[85] T. Wei, C. Chen, J. Hou, W. Xin, A. Mori, Nitric oxide induces oxidative stress and apoptosis in neuronal cells, Biochim. Biophys. Acta 1498 (2000) 72–79.
[86] C. Wu, T. Liu, W. Chen, S.-I. Oka, C. Fu, M.R. Jain, A.M. Parrott, A.T. Baykal, J. Sadoshima, H. Li, Redox regulatory mechanism of transnitrosylation by thioredoxin, Molecular & Cellular Proteomics 9 (2010) 2262–2275.
[87] C. Wu, A.M. Parrott, C. Fu, T. Liu, S.M. Marino, V.N. Gladyshev, M.R. Jain, A.T. Baykal, Q. Li, S. Oka, J. Sadoshima, A. Beuve, W.J. Simmons, H. Li, Thioredoxin 1-mediated post-translational modifications: reduction, transnitrosylation, denitrosylation, and related proteomics methodologies, Antioxid Redox Signal 15 (2011) 2565–2604.
[88] Y. Xu, F. Li, L. Lv, T. Li, X. Zhou, C.-X. Deng, K.-L. Guan, Q.-Y. Lei, Y. Xiong, Oxidative stress activates SIRT2 to deacetylate and stimulate phosphoglycerate mutase, Cancer Res. 74 (2014) 3630–3642.
[89] L. Yang, D. Wu, X. Wang, A.I. Cederbaum, Depletion of cytosolic or mitochondrial thioredoxin increases CYP2E1-induced oxidative stress via an ASK-1-JNK1 pathway in HepG2 cells, Free Radic Biol Med 51 (2011) 185–196.